

Improved analysis of strong-interaction-stable doubly-bottom tetraquarks on the lattice

B. Colquhoun,¹ A. Francis,² R. J. Hudspith,³ R. Lewis,⁴ K. Maltman,^{5,6} and W. G. Parrott⁴

¹*SUPA, School of Physics and Astronomy, University of Glasgow, Glasgow, G12 8QQ, UK*

²*Institute of Physics, National Yang Ming Chiao Tung University, 30010 Hsinchu, Taiwan*

³*GSI Helmholtzzentrum für Schwerionenforschung, 64291 Darmstadt, Germany*

⁴*Department of Physics and Astronomy, York University, Toronto, Ontario, M3J 1P3, Canada*

⁵*Department of Mathematics and Statistics, York University, Toronto, Ontario M3J 1P3, Canada*

⁶*CSSM, University of Adelaide, Adelaide, SA, 5005, Australia*

(Dated: July 15, 2024)

Abstract

We update earlier lattice results for the binding energies of the flavor antitriplet of strong-interaction-stable doubly bottom, $J^P = 1^+$ tetraquarks, employing an extended sink construction which produces significantly improved ground-state effective-mass plateaus, as well as new, larger-volume ensembles which reduce possible finite-volume effects at lighter pion masses. The updated bindings are 115(17) MeV for the $I = 0$ member of the antitriplet and 47(8) MeV for its $I = 1/2$ partner. We also provide an update of our earlier study of the variable heavy mass dependence of binding in the 1^+ channel and new results on this dependence for binding in the 0^+ channel, accessible when the two heavy quarks have unequal masses. Implications of these results of potential relevance to experimental searches for signals of the production of doubly bottom tetraquarks and/or a possible bottom-charm partner of the T_{cc} are also discussed.

I. INTRODUCTION

It has long been known that strong-interaction-stable manifestly exotic doubly-antiheavy-doubly-light tetraquark states exist in QCD in the limit of arbitrarily large heavy quark mass [1–3]. The source of this binding is the color Coulomb interaction between heavy antiquarks in a color 3_c configuration, which produces a binding contribution proportional to the reduced mass of the heavy antiquark pair. Additional attraction is present in channels where the accompanying light degrees of freedom (which necessarily have color $\bar{3}_c$) are in the flavor antisymmetric, color $\bar{3}_c$, light-quark spin $J_l = 0$ “good light diquark” configuration, known to be attractive from the observed splittings in the heavy baryon spectrum. Neither the heavy antiquark color-Coulomb attraction nor the spin-dependent, good-light-diquark attraction are accessible to a system of two well-separated heavy mesons. The doubly heavy channels most favorable to tetraquark binding are thus those with $J^P = 1^+$ and either $I = 0$ (light quark flavor ud) or $I = 1/2$ (light quark flavor ls , with $l = u, d$) for the case of identical heavy antiquarks, and $J^P = 0^+$ or 1^+ and either $I = 0$ or $I = 1/2$ for the case of non-identical heavy antiquarks. The discussion below focuses on these channels.

While bound doubly heavy tetraquark states necessarily exist for sufficiently large heavy antiquark mass,¹ whether the physical \bar{b} and \bar{c} masses are large enough for this binding to be realized in nature is a dynamical question. Since the heavy antiquark reduced mass, and hence the 3_c color Coulomb attraction, decreases with decreasing heavy quark mass, one expects such binding, if any, to be largest in doubly bottom channels. Numerous studies using QCD-inspired models predict binding in the doubly bottom $I = 0, J^P = 1^+$ channel, with additional doubly heavy bound states predicted in other channels in a number of these works [1, 2, 13–39]. The possibility of bound, doubly heavy tetraquarks has also been investigated in heavy-quark-symmetry-based approaches [3, 40–43] as well as in implementations of the Borel-transformed QCD sum rule framework employing the approximate, single-narrow-resonance-plus-OPE-continuum SVZ ansatz [44, 45] for the relevant spectral functions [46–55]. The sum rule analyses produce much larger errors for the ground state masses, with, in addition, results from different groups not in agreement, even within these larger errors, for a number of the channels. This situation is reviewed in more detail in Ref. [56].

Recent lattice studies exist for all of the doubly bottom, bottom-charm and doubly charm channels. All analyses concur on the existence of deeply bound strong-interaction-stable doubly bottom, $I = 0, J^P = 1^+$ [56–73] and $I = 1/2, J^P = 1^+$ [56, 60, 61, 64, 65, 68, 69, 72, 73] states. The situation is less clear for the $I = 0, J^P = 0^+$ and 1^+ bottom-charm channels. Refs. [56, 64, 65, 68, 69, 74] find finite-volume ground-state energies near or just above threshold and hence no deep binding, but are unable to rule out the possibility that these correspond to weakly bound states in the continuum. Ref. [75], in contrast, found a preliminary result of $\sim 20 - 40$ MeV for binding in the 1^+ channel, though with the caveat that a finite-volume study would be required to determine whether this represented a true continuum bound state signal. A Lüscher scattering analysis employing only ground-state energies as input and ensembles with partially quenched valence $m_\pi \gtrsim 500$ MeV [76], also reports an extrapolated physical-point $B^* \bar{D}$ scattering length corresponding to a 1^+ binding of $43 \begin{pmatrix} +7 \\ -6 \end{pmatrix} \begin{pmatrix} +24 \\ -14 \end{pmatrix}$ MeV. The analogous study of the 0^+ channel by the same authors [77], found a physical-point $B \bar{D}$ scattering length corresponding to $39 \begin{pmatrix} +6 \\ -4 \end{pmatrix} \begin{pmatrix} +18 \\ -8 \end{pmatrix}$ MeV 0^+ binding. A more recent Lüscher scattering analysis [78], however, with significantly lighter $m_\pi \simeq 220$

¹ see [4–12] for (early) lattice studies in this direction.

MeV and larger operator basis (including operators designed to have improved overlap with continuum meson-meson scattering states), on two $a \simeq 0.12$ fm ensembles with different volumes, finds instead very weakly bound genuine bound states (though compatible within statistical errors with being virtual bound states) 2.4(2.9) and 0.5(9) MeV, respectively, below $B^*\bar{D}$, respectively $B\bar{D}$, threshold in the $I = 0$, $J^P = 1^+$ and 0^+ channels.

In the doubly charmed sector, the 2021 LHCb discovery of the T_{cc} [79, 80] established the existence of a very weakly bound doubly charmed $I = 0$ state lying essentially right at DD^* threshold. This observation was in keeping with expectations from then-recent lattice studies, with Ref. [81] providing compelling evidence against the existence of a doubly charmed $I = 0$ $J^P = 1^+$ state with significant binding at the heavier-than-physical pion mass $m_\pi = 391$ MeV, and the results of the variable- b -mass study of Ref. [82], in combination with the negative bottom-charm results of Ref. [56], disfavoring the possibility of significant binding at physical m_π . The only lattice study leaving open the possibility of a moderately bound doubly charmed $I = 0$, $J^P = 1^+$ tetraquark had been that of Ref. [61], which reached m_π as low as 257 MeV for the coarsest of the three ensembles considered, and found a $J^P = 1^+$, $I = 0$ ground state lying 23 ± 11 MeV below DD^* threshold, though with no additional state (such as might correspond to the continuum DD^* threshold scattering state) nearby. As the authors noted, given the proximity of the two-meson threshold, a dedicated finite-volume study would have been required to clarify whether this result reflected the existence of an actual weakly bound ground state or, instead, corresponded to a continuum scattering state shifted below threshold by finite volume effects. The mass of the doubly charmed, strange, $I = 1/2$, $J^P = 1^+$ ground state in this study was also found to correspond within errors to that of the lowest-lying two-meson threshold, D^*D_s [61]. With the weakness of binding in the T_{cc} channel established experimentally, lattice efforts in this channel have turned to dedicated finite-volume scattering studies [83–88]. These studies, mostly at heavier-than-physical m_π , clearly establish the attractive nature of the $I = 0$ $J^P = 1^+$ DD^* interaction and agree on the existence of genuine or virtual DD^* bound states just below DD^* threshold for the m_π considered, in semi-quantitative agreement with LHCb results. Additional studies at lighter m_π and on finer lattices are expected in the near future.

As discussed in Ref. [56], existing lattice results rule out all implementations of the chiral quark model framework we are aware of in the literature. Predictions from a number of non-chiral models [13, 14, 16, 17, 19, 21–23, 25, 26, 29, 32, 34, 37–39], in contrast, are in reasonable agreement with existing lattice results, and would require improved lattice determinations to test them further. The heavy-quark-symmetry analyses of Refs. [42, 43], which rely on phenomenological input for leading finite heavy mass corrections, including model [42], respectively lattice [43], results for doubly heavy baryon masses not yet measured experimentally, also predict binding only in the two doubly bottom channels, with no binding of bottom-charm or doubly charmed states.

While recent lattice studies concur on the existence of an $SU(3)_F$ antitriplet of bound, strong-interaction-stable, doubly bottom $J^P = 1^+$ tetraquarks, results for the physical-point-extrapolated binding energies show some disagreements. In the $I = 0$ channel, two wall-source, local-sink studies from 2016 and 2018, Ref. [60] and [61], quote 189 ± 10 MeV and 143 ± 34 MeV, respectively, compatible with the result of the later study, Ref. [63], which found 189(18) MeV from the finest ensemble and 167(19) MeV averaged over all three ensembles considered. These results, however, are significantly higher than those of other recent lattice studies, with Ref. [62] reporting 128 ± 26 MeV, the preliminary one-ensemble $m_\pi \simeq 192$ MeV study of Ref. [56] ~ 113 MeV, Refs. [66, 67] 103(8) MeV, the HAL QCD study

of Ref. [89] 83(10)(20) MeV, Ref. [71] 112(13) MeV and Ref. [73] 100(10) $\left(\begin{smallmatrix} +43 \\ -30 \end{smallmatrix}\right)$ MeV. The situation is similar in the $I = 1/2$ channel where binding energies 46(12) MeV and 30(3) $\left(\begin{smallmatrix} +31 \\ -11 \end{smallmatrix}\right)$ MeV, found in the two most recent studies [71] and [73], are significantly lower than those of other recent lattice studies, which produced results 98(7) MeV [60], 87(32) MeV [61], a preliminary result $\sim 100(40)$ MeV [64], and 86(22)(10) MeV [65, 74]. A preliminary result, ~ 36 MeV, also favoring a lower value for the binding was also obtained in the multi-channel, but single-ensemble ($m_\pi \simeq 192$ MeV) study of Ref. [56].

The most deeply bound of the lattice results for the binding in the doubly bottom, $J^P = 1^+$, $I = 0$ and $I = 1/2$ channels, those of Ref. [60], came from an analysis using gauge-fixed wall sources and local sinks. Effective masses in such “wall-local” analyses typically approach the asymptotic ground state plateau from below, signalling negative excited state contamination. The fact that the ground state plateaus in this analysis were short, and reached at later Euclidean times, raised the possibility that the ground state masses were underestimated, and hence the associated bindings overestimated. This possibility was investigated in Ref. [56], at a single m_π ($\simeq 191$ MeV), using an improved “Box-Sink” construction designed to reduce excited-state contamination. The construction was shown to extend the ground state effective mass plateaus to much earlier Euclidean times and to significantly improve the ground state mass determinations. The results of that study confirmed that, at the single m_π considered, the $I = 0$ and $I = 1/2$ binding energies were indeed overestimated in Ref. [60]. A similar conclusion was reached in Ref. [71], also employing improved sink-side operators, designed to have better ground state overlap. For the $I = 0$ channel, this conclusion is in keeping with the result obtained in Ref. [62], which included two non-local “scattering operators” (products of two heavy-meson-like operators each projected to zero spatial momentum), though on the source side only, to avoid having to compute all-to-all propagators. These operators were expected to have improved overlap with the threshold BB^* scattering state (presumably the first excited state in the channel), and hence, as a result, to also improve the ground-state signal. These expectations were born out by the pattern of relative overlaps of the source operators with the lowest few GEVP Eigenstates. Refs. [66, 67, 73] took further advantage of this improvement by including the non-local scattering operators at the sink as well as at the source, producing a reduced error on the ground-state $I = 0$ binding energy. In this paper, we follow the alternate strategy of employing sink-side operators designed specifically to improved overlap with the ground state, extending the improved box-sink analysis of Ref. [56] to ensembles with a range of m_π , allowing an extrapolation of the results for binding in the doubly bottom, $J^P = 1^+$, $I = 0$ and $I = 1/2$ channels to physical m_π . Preliminary versions of this analysis were reported in Refs. [68, 69]. We also revisit the variable heavy mass study of Ref. [82] using the improved box-sink construction, and consider implications of the updated results for possible tetraquark binding in the $J^P = 1^+$ bottom-charm channel.

In light of the above discussion, we focus on doubly heavy states containing two heavy antiquarks, \bar{Q} and \bar{Q}' , and two light valence quarks, q and q' , with Q, Q' either b or a variable-mass version thereof (denoted h), and qq' either ud or ls , with $l = u, d$. The compressed flavor notations $ud\bar{b}\bar{b}$, $ud\bar{b}\bar{h}$, $ud\bar{h}\bar{h}$, $ls\bar{b}\bar{b}$, $ls\bar{b}\bar{h}$ and $ls\bar{h}\bar{h}$ will be used throughout to refer to such states.

The rest of this paper is organized as follows. In Sec. II we detail improvements to our earlier analysis, Ref. [60], implemented in the current work, outlining, in particular, the box-sink construction introduced in Ref. [56]. Sec. III provides details of our lattice simulations, including information on new, larger-volume ensembles. These ensembles allow us to reach near-physical m_π while keeping $m_\pi L > 3.6$. This provides better control over

possible finite volume effects than was the case in Ref. [60], where the ensemble with the lightest m_π had $m_\pi L = 2.4$. In Sec. IV, we present the results of these improved analyses for the binding energies of the doubly bottom, $J^P = 1^+$, $I = 0$ and $I = 1/2$ states together with an updated version of our earlier variable heavy mass study. A summary of these results, together with a discussion of possible implications for the $J^P = 1^+$ $ud\bar{b}\bar{c}$ channel, is provided in Sec. V.

II. IMPROVEMENTS TO THE PREVIOUS ANALYSIS

As in our previous study of the doubly bottom $J^P = 1^+$ channels [60], we work throughout with Coulomb gauge-fixed wall sources. The gauge condition has been implemented to high precision using the Fourier-accelerated conjugate gradient algorithm of Ref. [90] and applied over the full lattice volume. In order to avoid the larger errors noisier wall-wall correlators would have produced, our previous study, Ref. [60], employed local, rather than wall, sinks.

However, while source-sink symmetry ensures that excited state contributions enter wall-wall correlators with positive weights, and hence that ground state effective mass plateaus are approached from above, the effective masses for wall-local correlators typically approach their ground state plateaus from below, signalling negative amplitudes for at least the first excited state. When, as found in Ref. [60], ground state effective mass plateaus are short, and reached only at later Euclidean times, t , the possibility that the ground state signal has not yet fully plateaued leaves open the possibility that the ground state mass has been underestimated, and hence that, for channels in which the ground state is bound, the ground-state binding energy has been overestimated.

In Ref. [56] we addressed this issue by introducing the “box sink” construction. In contrast to a wall-wall correlator, which is constructed using propagators, $S^W(t)$, obtained by summing over the spatial sites of the sink time slice,

$$S^W(t) = \sum_x S(x, t) \quad (1)$$

a “wall-box” correlator is constructed using propagators obtained by restricting the sum to points lying within a specified radius, R , of the reference sink point, x . The resulting propagators have the form

$$S^{B;R}(x, t) = \frac{1}{N} \sum_{r^2 \leq R^2} S(x + r, t), \quad (2)$$

and, as R^2 is varied between the minimum and maximum values, 0 and $3L^2/4$, produce wall-box correlators which interpolate continuously between the wall-local and wall-wall limits [56]. The construction is predicated on the expectation that a range of intermediate R should exist for which excited-state contamination will be intermediate between the positive contamination of wall-wall correlators and negative contamination of wall-local correlators. Excited-state contamination should then be small, producing ground-state effective-mass plateaus that extend to considerably lower Euclidean t . One would expect a box-sink radius of roughly physical ground-state hadron size to optimize this improvement. Both this expectation, and the existence of significantly extended ground-state effective-mass plateaus, were confirmed in the single-ensemble study of Ref. [56]. The connection of this method to sink smearing was further elucidated in [91].

Other improvements to our earlier analyses are as follows. In our initial study, Ref. [60], we employed three $a \simeq 0.09$ fm, $32^3 \times 64$ Wilson-clover ensembles, generated by the PACS-CS collaboration, having pion masses ~ 164 , 299 and 416 MeV [92, 93]. $m_\pi L$ is > 4 for the latter two ensembles, but uncomfortably low (~ 2.4) for the ensemble with the lightest pion mass. We also restricted ourselves to a two-operator basis, and hence a 2×2 GEVP analyses. To ensure that potential finite-volume effects are under better control at lighter pion mass, and to improve the reliability of the extrapolation to physical m_π , we have generated additional, larger-volume, $48^3 \times 64$ ensembles at the same lattice spacing, with pion masses ~ 191 and ~ 165 MeV corresponding to $m_\pi L = 4.2$ and $m_\pi L = 3.6$, respectively. To more fully map out the light-quark mass dependence of the doubly bottom channel binding energies, we have also carried out box-sink analyses of two additional PACS-CS ensembles with heavier pion masses, ~ 575 and 707 MeV, in addition to the box-sink updates of our earlier analyses of the three previously studied $32^3 \times 64$ PACS-CS ensembles. Finally, to help better determine the ground-state signal, we have expanded our operator bases beyond the two-operator basis used in [60], and hence the number of correlators entering our analyses, and we employ the box-sink analysis described above (Eq. (2)) to all operators. We also perform multi-exponential fits in place of the GEVP previously used, which will be explained in detail below.

Table I provides details of the ensembles employed in this study, while further details of the operator bases used in the various channels are discussed below. Pion masses in Table I are obtained from multi-exponential fits, agreeing well with previous values obtained on these ensembles [94].

III. DETAILS OF THE LATTICE SIMULATIONS

A. Ensembles and correlator calculation

As noted above, our calculations are performed on nonperturbatively-improved Wilson-Clover PACS-CS ensembles [93], and additional ensembles generated as an extension to this set. All ensembles were generated with the same gauge action, β and c_{SW} , and we take the inverse lattice spacing to be $a^{-1} = 2.194(10)$ GeV as determined from the Ω mass at the

Label	V	κ_l	$N_{\text{conf}} \times N_{\text{src}}$	am_π	$m_\pi L$
E1	$32^3 \times 64$	0.13700	399×4	0.32205(18)	10.3
E2	$32^3 \times 64$	0.13727	400×4	0.26193(19)	8.4
E3	$32^3 \times 64$	0.13754	400×4	0.18960(29)	6.1
E5	$32^3 \times 64$	0.13770	800×4	0.13622(27)	4.4
E7	$48^3 \times 64$	0.13777	94×8	0.08719(47)	4.2
E9	$48^3 \times 64$	0.13779	88×4	0.07536(58)	3.6

TABLE I: Details of the lattice ensembles used in this study. The ensemble labels and volume, V (in lattice units), are given, as well as κ_l values, the statistics in terms of configurations and sources per configuration, the pion mass in lattice units (am_π) and the $am_\pi L$, where L is the spatial extent in lattice units. In all cases $\kappa_s^{\text{sea}} = 0.13640$ and $\kappa_s^{\text{valence}} = 0.13666$ [95]. Inverse lattice spacing in each case has been determined to be $a^{-1} = 2.194(10)$ GeV from the Ω mass at the physical point [96].

physical point [96].

The configurations were generated using the HMC algorithm implemented in openQCD version 1.6, see [97, 98] and references quoted therein. This package includes a number of beneficial techniques: such as the deflated SAP solver [99], mass-preconditioning [100], chronological inversions [101], and multiple time-scale integrators. In this work we have extended the existing set of PACS-CS ensembles by generating configurations with the same action parameters albeit with larger spatial volumes, $L/a = 32 \rightarrow 48$, as well as new light quark masses. For consistency with PACS-CS the strange quark mass parameter is kept fixed at its PACS-CS value, $\kappa_s = 0.13640$, while adding two additional light quark values, $\kappa_l = 0.13777$ (E7) and 0.13779 (E9). The corresponding pion masses and $m_\pi L$ are listed in Table I. There are some algorithmic differences worth noting in our ensemble generation, compared to that of PACS-CS: For the strange quark, the RHMC [102] was used, as opposed to the PHMC [103]. In this work, the number of poles in the rational approximation was kept large to ensure a stable generation process and allow for the corresponding reweighting factors to be dropped for the level of accuracy needed. Additionally a Hasenbusch preconditioning chain [100] with four intermediate masses μ_i was used for the light quarks. This is similar to the PACS-CS setup, however, the μ_i are different and the last is set to zero $\mu_0 = 0$, therefore no light quark reweighting is required. Measurements were performed every 16 MDU for E7 and every 8 MDU for E9. For the light quark propagator inversions the deflated SAP solver supplied in the same software package [98] was used. For the heavy quarks we used the same tadpole-improved $O(v^4)$ prescription detailed in the Appendices of [56].

We will use the following meson operators in determining our heavy-light meson masses:

$$\mathcal{O}_H = (\bar{h}(x)\gamma_5 q(x)), \quad \mathcal{O}_{H^*} = (\bar{h}(x)\gamma_i q(x)), \quad (3)$$

where q will be either an l or s quark. As we treat the source (wall) and sink (box) differently this will naturally need to be incorporated in our notation.

For the $I = 0$, $J^P = 1^+$, $T_{ud\bar{b}\bar{b}}$ and $T_{ls\bar{b}\bar{b}}$ tetraquarks we use the same set of local operators as in Ref. [56], listed in Tab. I of that reference.

This same set (with b replaced by h) is used for the local operators of the double-variable-heavy-mass $T_{ud\bar{h}\bar{h}}$ and $T_{ls\bar{h}\bar{h}}$ channels. The operators for the $I(J^P) = 0(1^+)/0(0^+)$ and $\frac{1}{2}(1^+)/\frac{1}{2}(0^+)$ channels having one physical- b -mass and one variable-heavy-mass antiquark, $T_{ud\bar{b}\bar{h}}$ and $T_{ls\bar{b}\bar{h}}$, are obtained from the “ $udcb$ ” and “ $uscb$ ” rows of the same table by replacing the “ c ” (which in Ref. [56] denoted a relativistic charm antiquark) with h (denoting here a NRQCD heavy antiquark whose mass we allow to vary over a range including values both heavier and lighter than physical m_b).²

For all ensembles except E7 we have, for each sink operator, four box radii squared³. In lattice units, these are in the range 30-49 for the tetraquarks, and 16-49 for the mesons (for which we will only use one source and sink operator per box radius). Our strategy is to use multiple sinks in a simultaneous fit to reliably extract the ground- and excited-state energies, as will be detailed below.

² With NRQCD used for the heavy quarks, the variable heavy mass, m_h , must, of course, remain in the region of validity of the use of NRQCD. The range thus does not extend down to m_h as low as physical m_c .

³ Owing to limited resources, for E7 we only have two box radii squared.

B. Correlator fitting

We use a standard Bayesian fitting approach, as outlined in [104], to simultaneously fit meson and tetraquark two point correlation functions to a multi-exponential fit form,

$$C_2^{\mathcal{O}_{\text{src}}^i \mathcal{O}_{\text{snk}}^j}(t) = \sum_{n=0}^N a_n^{\text{src}_i} a_n^{\text{snk}_j} (e^{-E_n t} \pm e^{-E_n(T-t)}), \quad (4)$$

obtaining correlated values for the ground state energies E_0 , where T is the length of the (periodic) lattice in the time dimension. Our data contains different source and sink combinations, (see Sec. III A), and these translate into different values for the amplitudes $a_n^{\text{src/snk}}$, with a common set of energy levels E_n .

The fits are performed using the *corrfitter*, *lsqfit* and *gvar* python packages [105–107]. The software calculates two measures of the goodness of fit, the χ^2 per degree of freedom (d.o.f.), and the log of the Gaussian Bayes Factor, $\log(\text{GBF})$. A good fit should have a $\chi^2/\text{d.o.f.}$ close to unity. The $\log(\text{GBF})$ gives a measure of the likelihood that the fitting ansatz gave rise to the results. This measure is useful in relative comparisons of different fit ansatzes, and penalises over-fitting.

As described in Appendix D of [108], unless statistics are many times larger than the number of data points, a Singular Value Decomposition (SVD) cut is required in order to faithfully represent the uncertainties in fit results. In this analysis, our statistics are limited and so we use an SVD cut in our correlator fits. An SVD cut is a conservative move, increasing uncertainty in the final result to reflect poorly determined eigenvalues in the covariance matrix. The required cut, which we shall always use, is calculated by *gvar* [107], using the method described in [108]. A downside of applying an SVD cut is that it artificially reduces the χ^2 of the fit, so SVD noise [108] is added as a final test to ensure that the unbiased $\chi^2/\text{d.o.f.}$ is acceptable.

1. Variable fit parameters

There are several input parameters which we choose in our fits. The first is the number of exponentials, N , appearing in Eq. (4), which may be different for the mesons and tetraquarks ($N^{\text{mes}}, N^{\text{tet}}$). Next, once the correlators have been folded (they are either periodic or anti-periodic), we can discard data at early and late times by choosing t_{min} and t_{max} and working in the window $t_{\text{min}} \leq t \leq t_{\text{max}}$, where, again, t_{min} and t_{max} can be different for mesons and tetraquarks. The other fit parameters we must choose are the prior values $\mathcal{P}[\textit{parameter}']$ which must be provided for each a_n and E_n in Eq. (4). We estimate the ground state energy prior, $\mathcal{P}[E_0]$, using an effective mass calculation

$$M_{\text{eff}} = \lim_{t \rightarrow \infty} \cosh^{-1} \left(\frac{C_2(t-1) + C_2(t+1)}{2C_2(t)} \right), \quad (5)$$

and vary the uncertainty given to $\mathcal{P}[E_0]$ in the fit. Similarly, for the effective amplitude, we have

$$(a_0^{\text{src}} a_0^{\text{snk}})_{\text{eff}} = \lim_{t \rightarrow \infty} \frac{C_2(t)}{e^{-M_{\text{eff}} t}}, \quad (6)$$

where we can set all n $a_n^{\text{src}0}$ parameters in Eq. (4) to = 1 for any one of the source operators (in this case operator $\mathcal{O}_{\text{src}}^0$) without loss of generality. We are left with the parameters $\mathcal{P}[a_0^{\text{snk}j}]$, (for sink operators $\mathcal{O}_{\text{snk}}^j$) again with a variable uncertainty. We can then use these to find effective amplitudes for the other source operators, which we have not set to 1. The priors for excited state amplitudes $\mathcal{P}[a_{n \neq 0}]$ (we drop the ‘src’ and ‘snk’ label from now on) are another choice varied in our fit.

For the meson excited state energy splitting priors, with excited state splittings expected to be of order Λ_{QCD} , we take for $\mathcal{P}[E_{n \neq 0}^{\text{mes}}]$ the range 500 ± 250 MeV. Since, in contrast, tetraquark/two-heavy-meson excited states are expected to be very closely spaced, we take as our prior for these splittings the value 30 ± 30 MeV. In both cases logarithmic priors are used to ensure the splittings are positive. This means that the 99.7% confidence interval for the meson splitting prior is between 100 MeV and 2 GeV, while that for the tetraquark is between 1.5 and 600 MeV.

2. Binning

In each of our ensembles, we have correlator data on N_{cfg} uncorrelated configurations (see Table I). On each configuration, we take 4 (8 for E7) evenly spaced source times, t_0 , for the correlators. Furthermore, for the vector meson and 1^+ tetraquarks, all three spatial components are calculated. For the pseudoscalar meson there is of course only one component. For the purposes of this discussion, let’s assume this component is copied three times for each t_0 on each configuration, such that for each correlator, on each configuration, there are 12 (24 for E7) measurements, which are not necessarily uncorrelated.

To obtain averaged data and a full covariance matrix from N_s samples, we use *gvar* [107], which calculates the covariance matrix, and required SVD cut, as per appendix D of Ref. [108]. This method relies upon the different samples being uncorrelated in order to give a true measure of the uncertainties. For this reason, we would typically average (bin) the 12 measurements for each configuration above (which could be correlated), before calculating the covariance matrix with the resulting $N_s = N_{\text{cfg}}$ samples. However, if we can be sure that these 12 measurements are only weakly correlated, we can treat them as independent samples. This effective increase in statistics will not change the central value or uncertainties on individual correlators, but should lead to a better determination of the covariance matrix, and thus a lower SVD cut, ultimately leading to smaller uncertainties in final fit parameters. To test what size of bin is permissible, we bin the data in sets of size 1, 3, 6, 12, and 24, with 12 being the default⁴, and 24 produced by combining the results from pairs of adjacent configurations. For each bin size, we average the data and generate the covariance matrix. Then we take each timeslice of each correlator and compare the relative change in the uncertainties from the default case (bin size 12), which we know is uncorrelated. If the samples in the new binning regime are also uncorrelated, we would expect the relative change in uncertainty to form a Gaussian distribution, with a mean of zero. In the case that they are correlated, we would expect the average standard deviation to be significantly different from the default (uncorrelated) binning for different bin sizes.

Figure 1 shows this distribution of the change in relative uncertainty for binnings of size 1, 3, 6, and 24, relative to the default binning of 12 for $u\bar{d}b\bar{b}$ data on the E3 ensemble. We see that the mean of the distribution is largely unchanged for binnings of 3 or 6, while the

⁴ On E7, there are twice as many t_0 values, so 24 is the default.

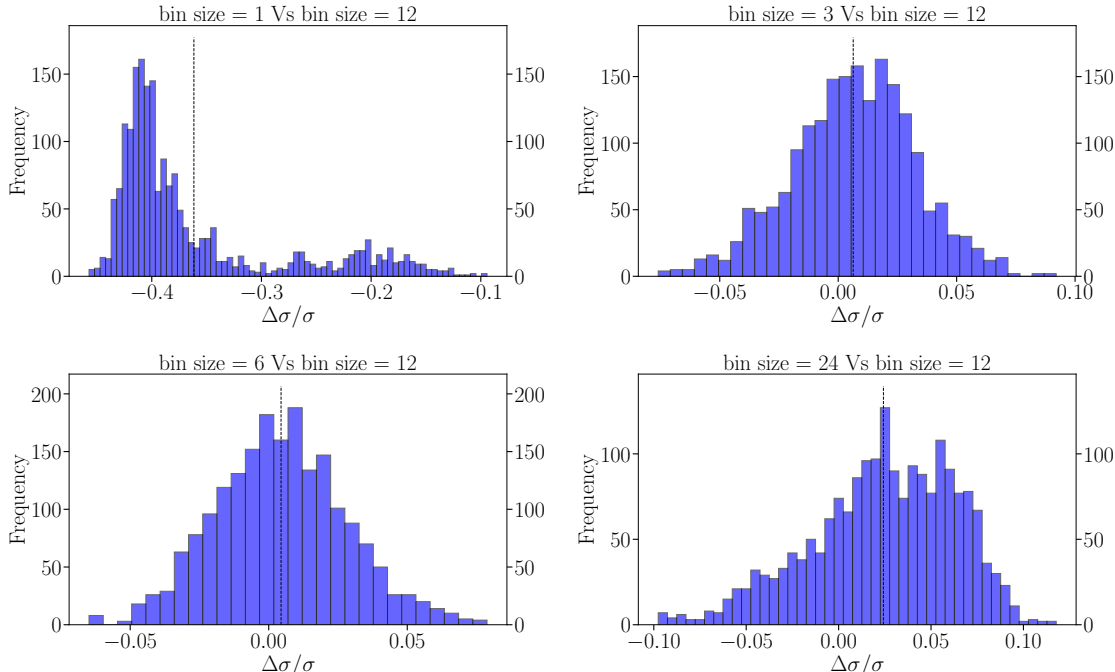


FIG. 1: The distribution of relative changes in uncertainty on correlators for binnings of size 1, 3, 6, and 24, relative to the default of 12. The black dotted line indicates the mean.

more conservative binning of 24 produces a mean increase of about 2% in uncertainty. For completeness, we include the binning of size 1, that is where individual vector components (or for the pseudoscalar 3 identical measurements) are treated as uncorrelated. As we expect, this results in a large decrease in uncertainty. All of our ensembles produce very similar results, where binnings of 3 or 6 would be acceptable. Taking a more conservative approach, we use a binning of 6 throughout, giving $N_s = 2N_{\text{cfg}}$ ($4N_{\text{cfg}}$ on E7). In our testing of fit stability, which will be described below, we check the effect of this binning on the final result.

3. Fitting strategy

The fitting strategy employed here on each ensemble is designed to be as thorough and agnostic as possible. First, taking just the mesons, we select a generous range of choices for the variable parameters discussed above, and perform a fit for all possible combinations of these choices. We then plot the resulting ground state energy, aM_{mes} , the $\chi^2/\text{d.o.f.}$ (recalling that these are artificially reduced by the SVD cut, so only meaningful in a relative sense), and the $\log(\text{GBF})$ for each of the fits, against each variable in turn, giving a spread of results for those choices of that variable. We then repeat exactly this process for just the tetraquarks. An example of such a plot in the tetraquark case, varying the number, N^{tet} , of exponentials for the $u\bar{d}\bar{b}\bar{b}$ fit on ensemble E1, is given in Fig. 2. In this case, we see that the central value of the mass (the dotted lines represent the averages of the displayed points) is relatively stable against changes in N^{tet} , but the χ^2 begins to grow below $N^{\text{tet}} = 7$. As expected, there is a larger relative uncertainty for larger values of N^{tet} . In this case, we can see that all $N^{\text{tet}} > 6$ are reasonable choices, with stable aM_{tet} values and small, stable χ^2 values. We select $N^{\text{tet}} = 7$, as it has the largest $\log(\text{GBF})$, suggesting that including further exponentials

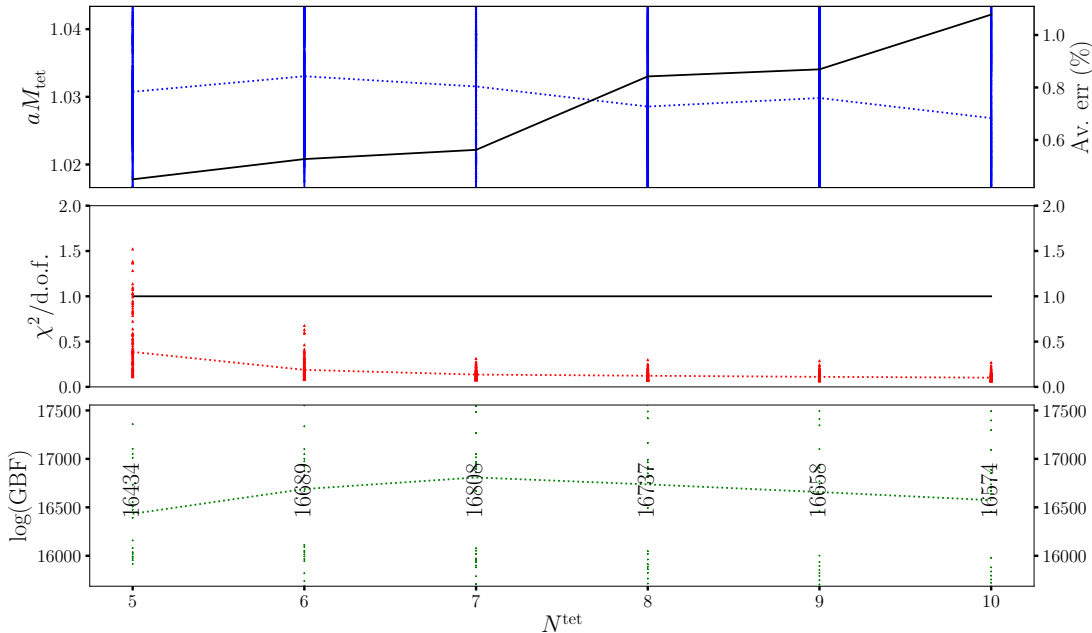


FIG. 2: Fit results for the $ud\bar{b}\bar{b}$ tetraquark ground-state mass as a function of N^{tet} on the E1 ensemble. The right-hand vertical axis and solid black line in the top panel give the corresponding mean relative uncertainty. The mean values (median for χ^2 and $\log(\text{GBF})$) are given by the dashed lines, with the value explicitly printed in the case of $\log(\text{GBF})$. The spread of the data reflects the variation of all other parameters.

beyond this would be over-fitting the data.

Once we have completed this process for the mesons and tetraquarks independently, we combine them in one simultaneous, correlated fit. There are now too many variable parameters to feasibly test all possible combinations, so we take the values we have already arrived at in the independent fits, and vary these one at a time. We check the stability of the result, and make changes to the choices if necessary (within the values which are acceptable from our above analysis), in order to find a fit which is stable. In general we found $ud\bar{b}\bar{b}$ fits to be much more stable than those for $ls\bar{b}\bar{b}$, likely due to the greater density of nearby threshold states in the latter.

Fig. 3 shows the results of this exploration for the $ls\bar{b}\bar{b}$ channel on the E3 ensemble. A list of the quantities varied is provided in the caption. The fit is seen to display good stability with respect to these variations, with generally small induced shifts in the $\chi^2/\text{d.o.f.}$ and $\log(\text{GBF})$, except when either the number of exponentials, N , or the uncertainty on a prior, is too small. In the figure, we display such variations for completeness, even when the increases in $\log(\text{GBF})$ they have produced are relatively large. The figure also includes the results for the splittings of the first excited tetraquark state, $aE^1 - aE^0$. The priors for these splittings are logarithmic to enforce positive splittings, which results in the asymmetric error bars shown. In this case, the error bars for $1(2)\sigma$ (i.e. the 68% and 95% confidence limits) are shown in black (red) and the binding energy is included in blue for comparison.

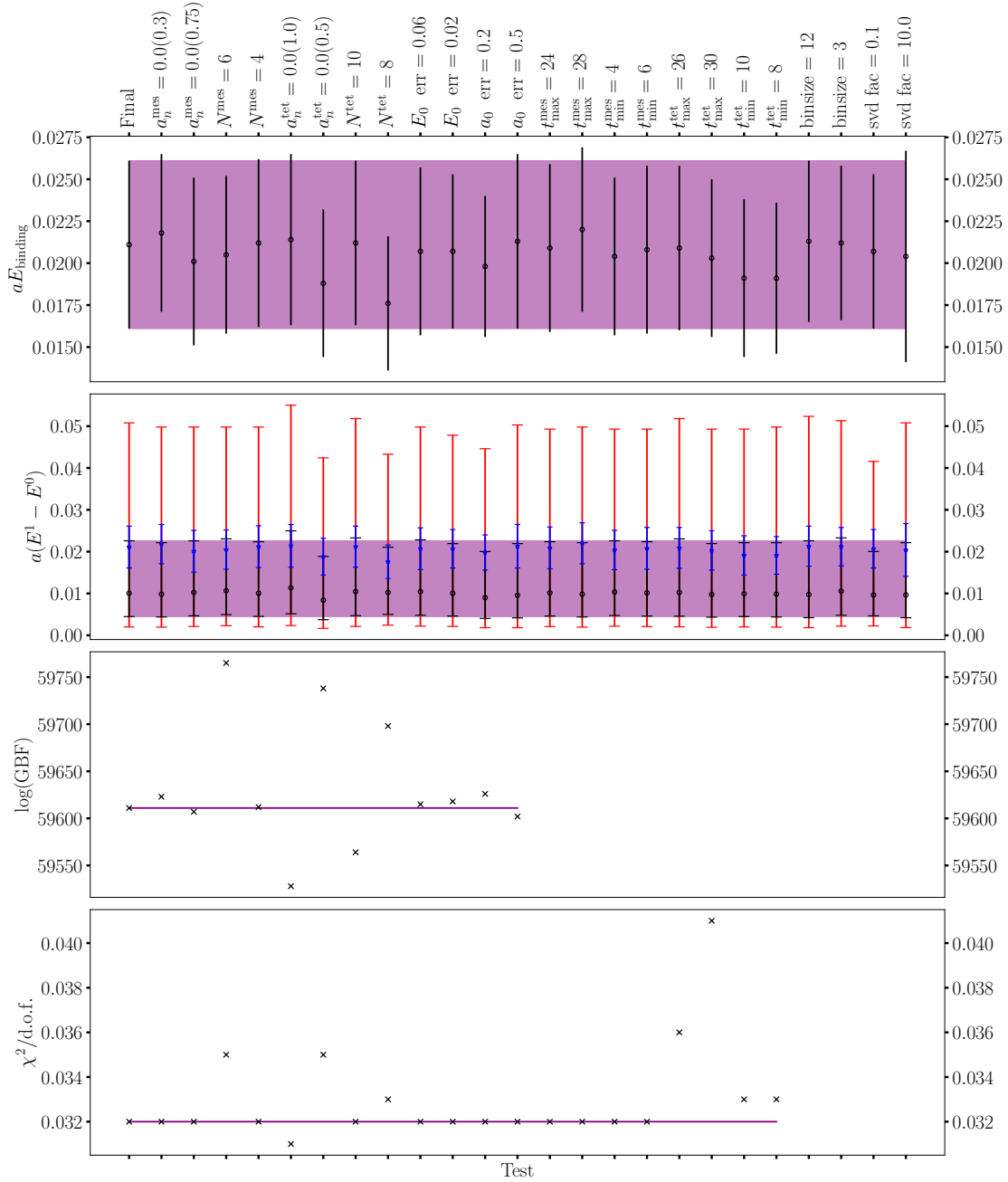


FIG. 3: Stability tests for $ls\bar{b}b$ on ensemble E3. We vary all parameters discussed in Sec. III B 1, one at a time, both increasing and decreasing them. ‘Final’ is our final fit result. We vary the number of exponentials, N , the priors $\mathcal{P}[a_{n \neq 0}]$ (labelled a_n), and the relative uncertainty on $\mathcal{P}[a_0]$ (Eq. (6), labelled a_0 err) and $\mathcal{P}[E_0]$ (Eq. (5), labelled E_0 err). We also change $t_{\min/\max}$, change the bin size, (see Sec. III B 2) and, finally, multiply the recommended SVD cut by 0.1 and 10, respectively. Note that $\log(\text{GBF})$ is not plotted for some tests, as the relative values are meaningful only when the raw data is unchanged. Similarly, χ^2 is affected by changes to the SVD cut and is only meaningful relatively. We plot the binding energy, and the gaps between the ground and first excited state, showing the $1(2)\sigma$ error bars in black (red). In the case of this first splitting, $a(E^1 - E^0)$, the binding energy from the row above is included in blue for comparison.

4. $ud\bar{h}\bar{h}$, $lsh\bar{h}$, $ud\bar{b}\bar{h}$ and $ls\bar{b}\bar{h}$ fits

In updating the earlier study [82] of the heavy-quark-mass dependence of tetraquark binding, we follow Ref. [82] and employ the highest-statistics ensemble available, E5, which has $m_\pi = 299$ MeV and $m_\pi L = 4.4$. The approach followed is similar to that described above, though with some modifications required to handle the larger data set that results from the variation of the heavy-quark mass. We begin by performing a stability analysis identical to that above, for each tetraquark channel and each heavy am_h value in turn, determining the corresponding bindings from stable versions of these individual fits. As we ultimately wish to fit the $ud\bar{h}\bar{h}$, $ud\bar{b}\bar{h}$, $lsh\bar{h}$ and $ls\bar{b}\bar{h}$ binding energies for different am_h to a fit form with common parameters, we would ideally like to fit all of the tetraquark correlators, for all am_h , together with the corresponding threshold meson correlators in one large, correlated fit. However, we find that, owing to its large size, such a combined fit is not feasible. To break it up, we first performed a number of tests examining the strength of correlations between different fit parameters. We found it possible to perform a simultaneous fit for the doubly heavy 1^+ $ud\bar{h}\bar{h}$ tetraquark and associated heavy meson, H and H^* , channels for all am_h . The maximum correlation between $ud\bar{h}\bar{h}$ bindings, $\Delta E(am_h)$, in this fit was found to be 0.12, with most correlations roughly 0.05. It is reasonable to assume the correlations between am_h -dependent tetraquark bindings in the other (singly heavy and/or strange) tetraquark channels will be similarly small. Next, for each am_h , we performed a simultaneous fit to extract $aM_{ud\bar{h}\bar{h}}$, $aM_{ud\bar{b}\bar{h}}$, aM_H and aM_{H^*} . Correlations between meson and tetraquark masses were found to be small ($\lesssim 0.1$), but those between $aM_{ud\bar{h}\bar{h}}$ and $aM_{ud\bar{b}\bar{h}}$ were more significant (typically ≈ 0.25). Similar results were found for the ls analogues. These inter-tetraquark correlations are further enhanced when we turn from the tetraquark masses to the corresponding binding energies, where the effect of shared threshold meson masses comes into play and we find correlations between the bindings of $ud\bar{h}\bar{h}$ and $ud\bar{b}\bar{h}$ tetraquarks of $\gtrsim 0.5$ (and similarly for $lsh\bar{h}$ and $ls\bar{b}\bar{h}$).

Based on these observations, we adopt the following strategy. First, we simultaneously fit all meson correlators for all am_h to extract aM_H , aM_{H^*} , aM_{H_s} and $aM_{H_s^*}$. These will be taken in various combinations to provide the two meson thresholds for each tetraquark. Second, we simultaneously fit all tetraquarks for *each* am_h to extract $aM_{ud\bar{h}\bar{h}}$, $aM_{ud\bar{b}\bar{h}}$, $aM_{lsh\bar{h}}$, $aM_{ls\bar{b}\bar{h}}$. This ensures we have fits which are tractable, while also preserving correlations where they are significant. Finally, we ensure that the resulting bindings from this correlated method agree with those found when we optimised and stabilised the individual am_h fits above.

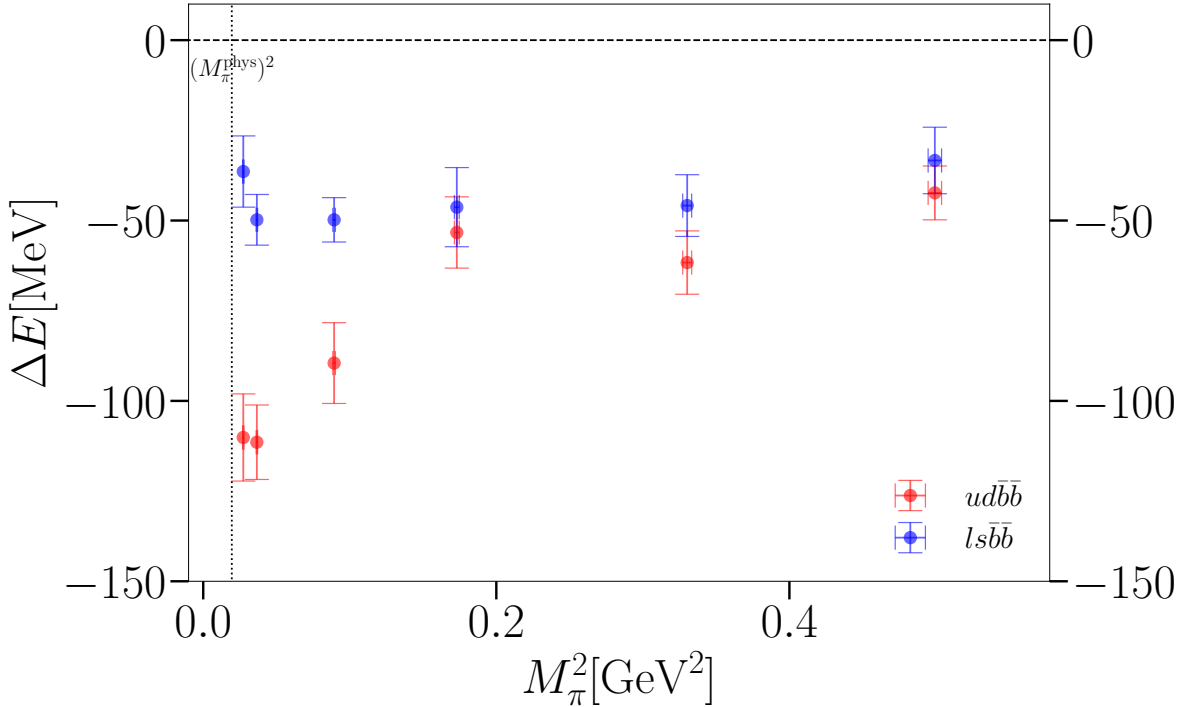
IV. RESULTS

A. Light-quark mass dependence and the physical-point $ud\bar{b}\bar{b}$ and $ls\bar{b}\bar{b}$ binding energies

Numerical results for the binding energies of the $J^P = 1^+$ $ud\bar{b}\bar{b}$ and $ls\bar{b}\bar{b}$ tetraquarks on the six ensembles studied are presented in Table II, and plotted as a function of m_π^2 in Fig.4. Results are given in lattice units and MeV.

To extrapolate these results to physical m_π , we employ fits with the expected leading linear-in- m_π^2 chiral behavior and, as in Ref. [71], a finite volume (FV) term exponential in

m_π [MeV]	$-a\Delta E_{ud\bar{b}\bar{b}}$	$-a\Delta E_{ls\bar{b}\bar{b}}$	$-\Delta E_{ud\bar{b}\bar{b}}$ [MeV]	$-\Delta E_{ls\bar{b}\bar{b}}$ [MeV]
707	0.0193(34)	0.0152(42)	42.3(7.5)	33.3(9.2)
575	0.0281(40)	0.0209(39)	61.7(8.8)	45.9(8.6)
416	0.0243(45)	0.0211(50)	53.3(9.9)	46(11)
299	0.0408(51)	0.0227(28)	90(11)	49.8(6.1)
191	0.0508(47)	0.0227(32)	111(10)	49.8(7.0)
165	0.0502(55)	0.0166(45)	110(12)	36.4(9.9)

TABLE II: Binding energies in the $J^P = 1^+$ $ud\bar{b}\bar{b}$ and $ls\bar{b}\bar{b}$ channels as a function of m_π .

FIG. 4: Tetraquark binding in the $J^P = 1^+$ $ud\bar{b}\bar{b}$ and $ls\bar{b}\bar{b}$ channels versus m_π^2 for $m_\pi \approx 700, 575, 415, 299, 192$ and 165 MeV.

$m_\pi L$, where L is the spatial extent of the lattice. The resulting fit form is

$$a\Delta E = A_0(1 + A_1(am_\pi)^2 + A_2e^{-m_\pi L}), \quad (7)$$

with the physical result recovered by setting $m_\pi \rightarrow m_\pi^{\text{phys}}$ and $L \rightarrow \infty$. We have made a explicit for clarity, noting that all A s are dimensionless⁵. For A_2 , the range of $m_\pi L$ for the ensembles we consider extends down only to $\simeq 3.6$, giving us limited leverage for fitting FV effects and preventing a meaningful fit for this quantity. Since a significantly wider range of $m_\pi L$, extending down to $\simeq 2.7$, was available to the authors of Ref. [71], we have used the results of the fit from that reference, provided to us by the authors, as priors for our fit, taking $A_2 = -3.1(7)$ in the $ud\bar{b}\bar{b}$ case.⁶ With our $m_\pi L$ values in the range 3.6 to 10.3, this

⁵ We perform the fit in lattice units to avoid D'Agostini (normalisation) bias [109]. Results are converted to physical units after fitting.

⁶ We thank the authors of for providing us with this information, which was not explicitly quoted in Ref. [71].

turns out to give only a modest correction to the final values. In the $ls\bar{b}\bar{b}$ case, we expect, in addition to somewhat smaller effects proportional to $e^{-m_\pi L}$, possible additional effects proportional to $e^{-m_K L}$. The former are dealt with by employing a FV term $A_2^{ls} e^{-m_\pi L}$ in the $ls\bar{b}\bar{b}$ analogue of Eq. 7, taking a conservative prior of 0(3) for A_2^{ls} . The latter are expected to be very small, and hence neglected, given the much larger values of $m_K L$ ($m_K L > 8.7$) for the ensembles considered. These fits are again carried out using *lsqfit* [106]. Since the range of pion masses considered extends up to $\simeq 707$ MeV, a value likely well beyond the range of validity of the fit ansatz Eq. (7), we perform a number of such fits, starting with one involving the two ensembles with m_π closest to the physical value (E7 and E9), and adding, one at a time, the ensemble with the next lightest m_π to the fit.

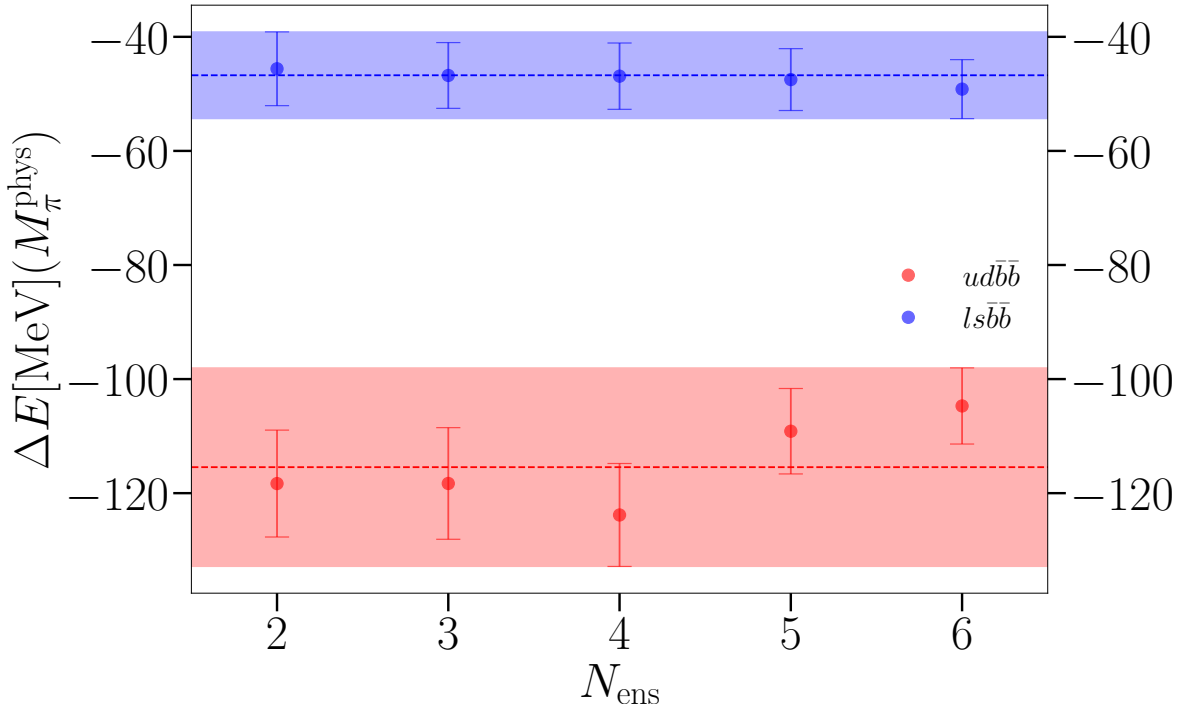


FIG. 5: Physical-point extrapolations of the 1^+ $ud\bar{b}\bar{b}$ and $ls\bar{b}\bar{b}$ binding energies from fits including N_{ens} ensembles (see text). Our final results are represented by the coloured bands.

Figure 5 shows the resulting extrapolated physical-point values of the 1^+ $ud\bar{b}\bar{b}$ and $ls\bar{b}\bar{b}$ binding energies, $\Delta E(M_\pi^{\text{phys}})$, as a function of N_{ens} , the number of ensembles included in the fit. The $ls\bar{b}\bar{b}$ binding is seen to be relatively independent of N_{ens} , while the $ud\bar{b}\bar{b}$ binding decreases by about a sigma once the two ensembles with the heaviest m_π are included.

While we expect the fits with smaller N_{ens} (and hence smaller maximum m_π) to be more reliable, to be conservative, we take as our final results in each channel those represented by the central values and half-widths of the colored bands shown in Fig. 5, which span the ranges covered by the error bars of all six such fits. These are

$$\Delta E_{ud\bar{b}\bar{b}}(m_\pi^{\text{phys}}) = -115(17) \text{ MeV} \quad (8)$$

$$\Delta E_{ls\bar{b}\bar{b}}(m_\pi^{\text{phys}}) = -46.7(7.6) \text{ MeV}. \quad (9)$$

The finite volume corrections described above (and included in Fig. 5 and Eqs. (8) and (9)) decrease the $\Delta E_{ud\bar{b}\bar{b}}(m_\pi^{\text{phys}})$ (i.e., deepen the binding) obtained for each N_{ens} by roughly

one standard deviation. The net effect is a final $ud\bar{b}\bar{b}$ binding, quoted in Eq. (8), 7 MeV ($\approx 0.4\sigma$) more bound, and with an uncertainty 3 MeV larger, than that obtained neglecting finite-volume corrections. For $\Delta E_{l\bar{s}\bar{b}\bar{b}}(m_\pi^{\text{phys}})$, the effects simply increase the uncertainties, without significantly changing the central values. The result is a final uncertainty in Eq. (9) 1 MeV larger than that obtained in the uncorrected case.

B. Heavy mass dependence

The heavy mass dependence of the binding, ΔE , for $ud\bar{h}\bar{h}$, $ud\bar{b}\bar{h}$, $l\bar{s}\bar{h}\bar{h}$ and $l\bar{s}\bar{b}\bar{h}$ tetraquarks is discussed at length in [82], with the underlying NRQCD implementation outlined in Appendix A of that paper. The variable, spin-averaged $\eta_h\text{-}\Upsilon_h$ mass is determined as a function of the input NRQCD parameter aM_Q by measuring the kinetic mass, with the ratio of the physical spin-averaged $\eta_b\text{-}\Upsilon_b$ mass to the resulting kinetic mass taken to define the ratio $r_h \equiv m_b/m_h$. We follow Ref. [82] in carrying out this study on the highest-statistics ensemble available, E5, which has $m_\pi = 299$ MeV and $m_\pi L = 4.4$. We also employ the phenomenological fit forms used in that paper, here recast using the notation $\delta_l = M_{B^*} - M_B$ and $\delta_s = M_{B_s^*} - M_{B_s}$ for the physical heavy bottom-meson splittings. As usual, with $M_{BB^*}^{\text{spin av.}}$ the spin average of the B and B^* masses, $M_B = M_{BB^*}^{\text{spin av.}} - \frac{3}{4}\delta_l$ and $M_{B^*} = M_{BB^*}^{\text{spin av.}} + \frac{1}{4}\delta_l$, with analogous expressions for M_{B_s} and $M_{B_s^*}$. These splittings set the overall scales of the $m_b/m_h \equiv r_h$ -dependent contributions to tetraquark binding in the various channels from heavy-light interactions in the associated two-meson threshold states, represented by the last terms in the expressions below. The mass-dependent factors accompanying the splittings in these expressions are determined by which two mesons form the two-meson threshold for the channel in question. For $ud\bar{b}\bar{h}$, for example, the threshold is B^*H for $m_h < m_b$ ($r_h > 1$) and H^*B for $m_h > m_b$ ($r_h < 1$).

With the above notation, the expressions of Ref. [82] for the singly-heavy, variable-mass 1^+ $ud\bar{b}\bar{h}$ bindings become

$$\begin{aligned} \Delta E^{\text{ud}\bar{b}\bar{h}} &= \frac{C_0}{r+r_h} + C_1^{rud} + C_2^{rud}(r+r_h) - \left(\frac{1}{4}r - \frac{3}{4}r_h\right)\delta_l \quad (r_h > 1) \\ \Delta E^{\text{ud}\bar{b}\bar{h}} &= \frac{C_0}{r+r_h} + C_1^{rud} + C_2^{rud}(r+r_h) - \left(\frac{1}{4}r_h - \frac{3}{4}r\right)\delta_l \quad (r_h < 1), \end{aligned} \tag{10}$$

where $r \equiv m_b/m_b = m_h/m_h = 1$, and the terms proportional to C_0 , C_1^{rud} , and C_2^{rud} serve to parameterize the attractive color Coulomb interaction between the two heavy antiquarks, the spin-dependent good-light-diquark attraction, and residual $1/m_h$ -dependent effects (such as differences in light-heavy interactions and heavy-quark kinetic energy between the tetraquark and two-meson threshold states), respectively.⁷ The apparently unnecessary notation r for quantities which are here identically equal to 1 is introduced for the purpose of compactness, allowing the corresponding forms for the doubly-heavy, variable-mass 1^+ $ud\bar{h}\bar{h}$ cases to be obtained by replacing all occurrences of r with r_h . For $l\bar{s}\bar{b}\bar{h}$, the lowest two-meson thresholds are B^*H_s for $r_h > 1$ and H^*B_s for $r_h < 1$, and the phenomenological forms for

⁷ The color Coulomb term in Eq. (10) is proportional to the reduced mass of the two heavy quarks, $\mu_{bh} = m_b m_h / (m_b + m_h) = m_b / [r_h + 1]$, with the factor of m_b in the numerator absorbed into the definition of C_0 . Similarly, the term proportional to C_2 reflects an assumed heavy-mass dependence of the form $(1/m_b) + (1/m_h) = (1/m_b)[1 + r_h]$, with the overall $(1/m_b)$ factor absorbed into C_2 .

the singly-heavy, variable-mass $1^+ \text{ls}\bar{\text{b}}\bar{\text{h}}$ bindings are

$$\begin{aligned}\Delta E^{\text{ls}\bar{\text{b}}\bar{\text{h}}} &= \frac{C_0}{r+r_h} + C_1^{ls} + C_2^{ls}(r+r_h) - \left(\frac{1}{4}\delta_l r - \frac{3}{4}\delta_s r_h\right) \quad (r_h > 1) \\ \Delta E^{\text{ls}\bar{\text{b}}\bar{\text{h}}} &= \frac{C_0}{r+r_h} + C_1^{ls} + C_2^{ls}(r+r_h) - \left(\frac{1}{4}\delta_l r_h - \frac{3}{4}\delta_s r\right) \quad (r_h < 1),\end{aligned}\tag{11}$$

with the corresponding doubly-heavy variable-mass forms again obtained by the replacement $r \rightarrow r_h$. The superscripts on the fit parameters $C_1^{ud,ls}$ and $C_2^{ud,ls}$ reflect the expected dependence of these quantities on the masses of the light quarks involved. This dependence also means that $C_1^{ud,ls}$ and $C_2^{ud,ls}$ will differ from ensemble to ensemble, with the results obtained from the fits of the current study specific to the E5 ensemble employed.

The fit forms above are predicated on the assumption that the binding in any deeply bound doubly heavy tetraquark system will be dominated by the combination of the attractive color-Coulomb interaction between two heavy antiquarks in a color 3_c configuration and the attractive spin-dependent good-light-diquark interaction known to be present in the static heavy-quark limit and reflected experimentally in the splittings in the singly heavy baryon spectrum. Additional contributions, resulting from deviations of non-color-Coulomb effects from their static values, are assumed to be numerically subleading, and parametrizable by the terms proportional to $C_2^{ud,ls}$. These assumptions will become less reliable as the heavy-quark mass decreases and one moves farther from the static limit. The fit forms are also expected to break down for weakly bound systems, where the wave-function will become dominated by longer-distance two-meson components, reducing the effect of the attractive short-distance interactions available in a more deeply bound, localized system. Note that the assumptions underlying these forms, if reliable, should satisfy some semi-quantitative self-consistency tests. For example, the strong increase in the strength of the attractive color-Coulomb interaction with increasing am_h expected in the $\text{ud}\bar{\text{h}}\bar{\text{h}}$ and $\text{ls}\bar{\text{h}}\bar{\text{h}}$ systems should show up when the heavy-quark mass is varied to values larger than am_b . Physically constrained expectations also exist for $C_1^{ud,ls}$, provided, as assumed, these are dominated by the known attractive good-light-diquark contribution. where we know, from the physical Σ_b - Λ_b splitting, that, relative to the spin average, the spin-dependent good-light-diquark attraction is $-3/4$ times the Σ_b - Λ_b splitting, or -145 MeV. One would thus expect a physically sensible fit form to produce a result $C_1^{ud} \simeq -145$ MeV for an ensemble with physical m_π and m_K . Similarly, from the physical Ξ'_b - Ξ_b splitting, a physically sensible fit form should produce a result $C_1^{ls} = \simeq -104$ MeV for an ensemble with physical m_π and m_K . With these physical-point results establishing the decrease of the good-light-diquark attraction with increasing light-quark mass, we further expect to find smaller negative values of C_1^{ud} and C_1^{ls} for ensembles with heavier-than-physical m_π , such as E5.

Correlated fits of the variable- r_h E5 data are carried out using *lsqfit* [106], which makes extensive use of *gvar* [107].

The results for the parameters δ_l and δ_s , obtained from the combined all- am_h fit for aM_H , aM_{H^*} , aM_{H_s} and $aM_{H_s^*}$, are $\delta_l = 41.7(2.7)$ MeV and $\delta_s = 45.8(1.7)$ MeV. These agree well with the PDG [110] values, $\delta_l = 45.42(26)$ MeV and $\delta_s = 46.1(1.5)$ MeV. Using the PDG values in place of the fit values has no significant impact on our results. As noted above, the aM_H , aM_{H^*} , aM_{H_s} and $aM_{H_s^*}$ results are used to determine the lowest two-meson thresholds needed for determining the tetraquark binding energies.

In Fig. 6, we present the results for the E5 ensemble $J^P = 1^+ \text{ud}\bar{\text{h}}\bar{\text{h}}$, $\text{ls}\bar{\text{h}}\bar{\text{h}}$, $\text{ud}\bar{\text{b}}\bar{\text{h}}$ and $\text{ls}\bar{\text{b}}\bar{\text{h}}$ tetraquark binding energies, together with colored bands showing the fit to these results

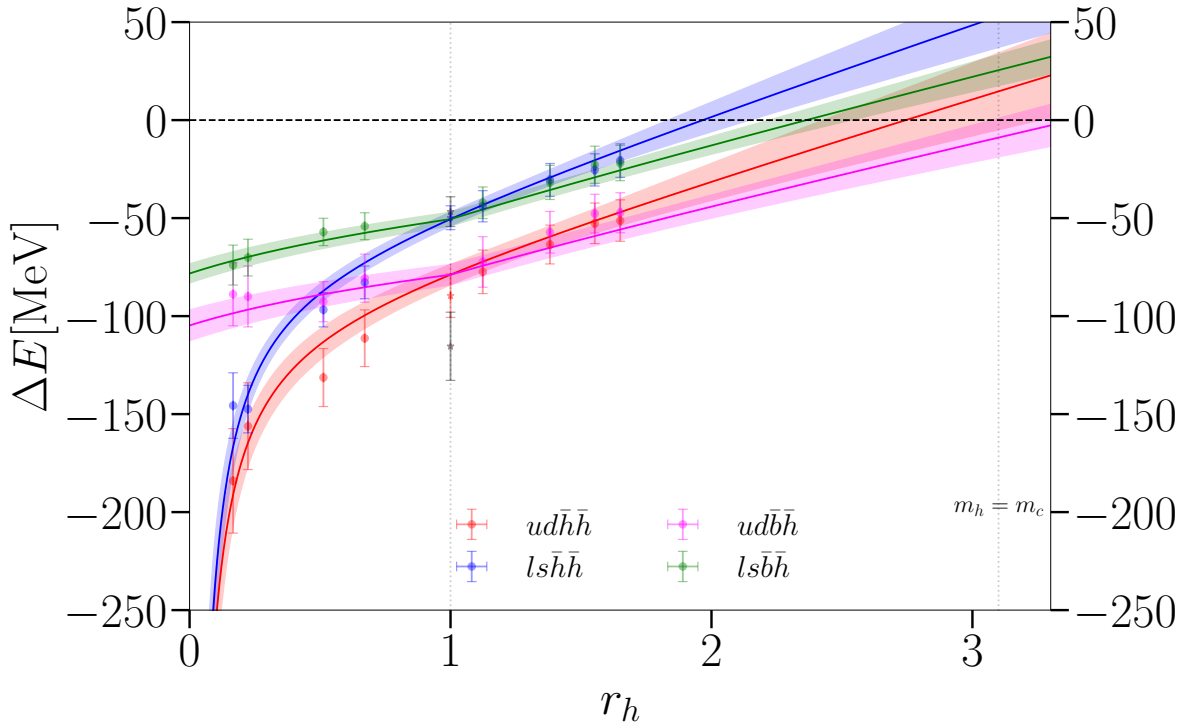


FIG. 6: Binding energies of $J^P = 1^+$ tetraquark states bound below the lowest two-meson threshold on the E5 ensemble, plotted against r_h . Coloured bands are the results of correlated fits to Eqs. (10) and (11). The points at $m_b/m_h = 1$ with the black error bars are the results of a physical-point continuum extrapolation, discussed below in Sec. IV A.

produced using the r_h -dependent phenomenological forms above. Table III gives the resulting fit parameter values, errors and correlations. The fit has a $\chi^2/\text{d.o.f.}$ of 0.55.

C_0	C_1^{rud}	C_2^{rud}	C_1^{ls}	C_2^{ls}
-31.8(6.3)	-102(14)	14.8(5.1)	-79(12)	16.7(4.2)
1.000	-0.558	0.411	-0.786	0.663
	1.000	-0.911	0.684	-0.573
		1.000	-0.525	0.506
			1.000	-0.930
				1.000

TABLE III: E5 ensemble $J^P = 1^+$ tetraquark fit results. Line 1: Fit results (in MeV) for the coefficients in Eqs. (10) and (11). Lines 2-6: the corresponding correlation matrix.

Immediately evident from the figure are the rapid increases in $ud\bar{h}\bar{h}$ and $l\bar{s}h\bar{h}$ binding with decreasing r_h (increasing am_h), associated with the unbounded growth of the color-Coulomb attraction in those cases as $r_h \rightarrow 0_+$ ($am_h \rightarrow \infty$). The fit results for C_1^{rud} and C_1^{ls} are also seen to be $\sim 20\%$ less attractive than the corresponding physical-point values, in keeping with the heavier-than-physical 299 MeV value of m_π on the E5 ensemble and the expectations discussed above. The good agreement of the phenomenological fits with the r_h -dependence of the lattice results clearly suggests the physical picture underlying the fit forms has succeeded in identifying the main sources responsible for the observed deep binding in the $u\bar{d}b\bar{b}$ and $l\bar{s}b\bar{b}$

tetraquark channels. While the region of reliability of the NRQCD heavy-quark treatment extends down only to $m_h \simeq 0.6m_b$ [82] ($r_h \simeq 1.7$), and hence does not reach $m_h = m_c$ ($r_c \simeq 3.1$), this suggests extrapolated versions of the fits (bearing in mind the additional ~ 45 (~ 25) MeV in good ud (ls) diquark binding expected for physical m_π based on the E5 results for C_1^{ud} and C_1^{ls}) may provide useful qualitative guides to what is expected as m_h is reduced further towards m_c . This conclusion is supported by the observation that a rough by-eye extrapolation of the NRQCD-based E5 $ud\bar{h}\bar{h}$ results to $r_h \simeq 3.1$, supplemented by the expected additional ~ 45 MeV in good-light-diquark-source binding at physical m_π for the points shown in the figure, leads to the expectation of a binding near zero in the physical 1^+ $ud\bar{c}\bar{c}$ tetraquark channel, an expectation compatible with the observed very weakly bound T_{cc} found by LHCb [79, 80]. The figure, further, suggests that (i) with binding in the 1^+ $lsh\bar{h}$ and $lsb\bar{h}$ channels always less than that in the $ud\bar{h}\bar{h}$ channel and the T_{cc} observed to lie essentially at threshold, no bound 1^+ state is expected in either of the $ls\bar{c}\bar{c}$ or $ls\bar{b}\bar{c}$ channels, and (ii) with the T_{cc} weakly bound and the fit showing binding in the 1^+ $ud\bar{b}\bar{h}$ channel greater than that in the 1^+ $ud\bar{h}\bar{h}$ channel for $r_h > 1$, a bound $ud\bar{b}\bar{c}$ tetraquark is likely to exist in the $I = 0$, $J^P = 1^+$ channel, albeit (given the preponderance of previous lattice results) with relatively small binding. The latter conclusion is in keeping with expectations based on (i) the results of the recent, slightly heavier-than-physical $m_\pi \simeq 220$ MeV lattice scattering study of Ref. [78], which found a genuine bound state (though compatible within statistical errors with being a virtual bound state) 2.5(2.9) MeV below $B^*\bar{D}$ threshold, and (ii) the anticipated small increase in binding due to increased good-light-diquark attraction at shorter $B^*\bar{D}$ separations expected at slightly lower, physical m_π . Weak binding in this channel is also compatible with the results of Refs. [56, 74] which, though showing no signs of deep binding, could not rule out a weakly bound state. The weak binding found in Ref. [78] shows some tension with the 43 $\begin{pmatrix} +7 \\ -6 \end{pmatrix}$ $\begin{pmatrix} +24 \\ -14 \end{pmatrix}$ MeV result of the mixed-action, overlap-valence on HISQ-sea study of Ref. [76], though the latter employs a small set of interpolating operators and results from a physical-point extrapolation from valence pion masses, 0.5, 0.6, 0.7, 1.0 and 3.0 GeV, significantly heavier than considered in Ref. [78]. The 1^+ $ud\bar{b}\bar{c}$ channel will be discussed in more detail in Sec. V.

In Figure 7 we plot results for tetraquark binding in the $J^P = 0^+$ $ud\bar{b}\bar{h}$ and $ls\bar{b}\bar{h}$ channels, channels in which tetraquark configurations without relative heavy-quark spatial excitation are possible when the two heavy quarks are different. Also shown for comparison are the corresponding 1^+ $ud\bar{b}\bar{h}$ and $ls\bar{b}\bar{h}$ results and associated phenomenological fit bands from Fig. 6. Tetraquark binding is found to be similar, within errors, in the 1^+ and 0^+ $ls\bar{b}\bar{h}$ channels. In contrast, 0^+ binding is found to be somewhat smaller than 1^+ binding in the $ud\bar{b}\bar{h}$ channel. The lattice scattering study of Ref. [78] also found a similar comparable, though somewhat reduced, binding in the 0^+ than the 1^+ $ud\bar{b}\bar{c}$ channel in a simulation with $m_h = m_c$ and $m_\pi \simeq 220$ MeV. Given that these scattering results, the results of Refs. [56, 74], and the qualitative extrapolation of the phenomenological fit to $m_h \simeq m_c$ all agree on at-most-weak-binding in the 1^+ $ud\bar{b}\bar{c}$ channel, these observations suggest that, while a deeply bound 0^+ $ud\bar{b}\bar{c}$ tetraquark would definitely exist were the charm quark to be sufficiently heavier than it is in nature, at physical m_c the 0^+ $ud\bar{b}\bar{c}$ state is likely either unbound or only weakly bound. In the case that the 0^+ $ud\bar{b}\bar{c}$ state is weakly bound, the weakness of both the 1^+ and 0^+ bindings ensures that the mass of the 0^+ state will be less than that of the corresponding 1^+ state. The consequences for a possible experimental $ud\bar{b}\bar{c}$ tetraquark signal of either this scenario or a scenario where the 1^+ state is bound but the 0^+ state is not are discussed in Sec. V below.

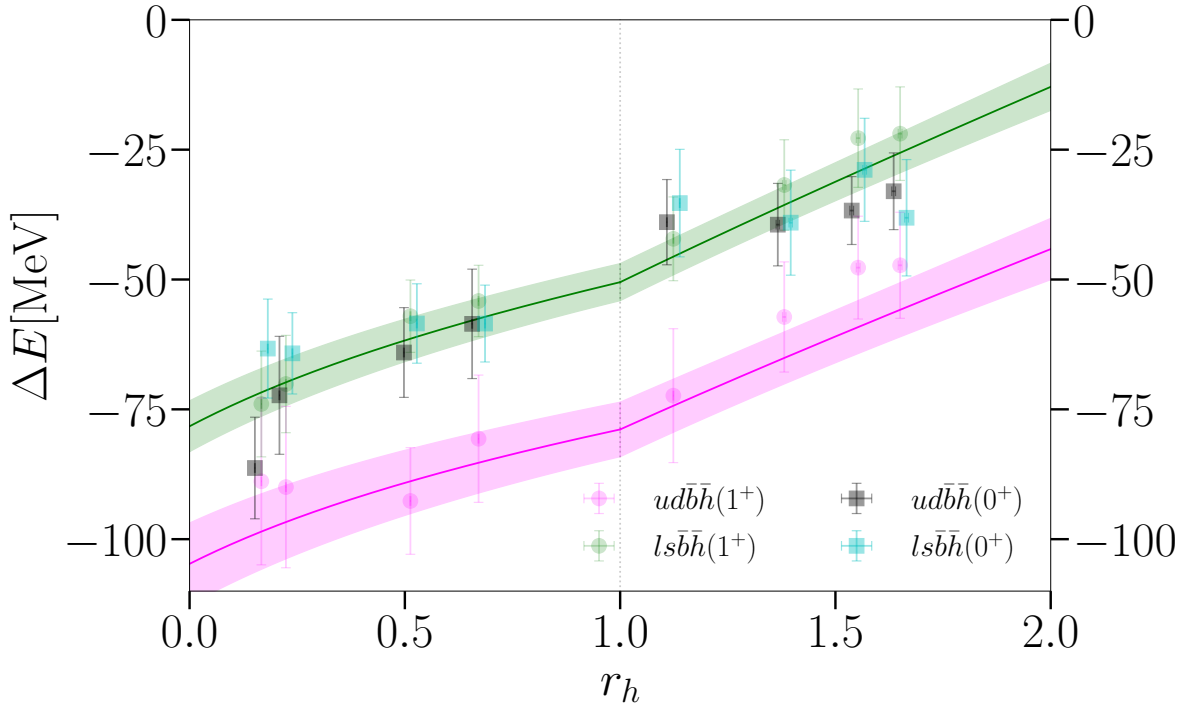


FIG. 7: Binding energies of $J^P = 1^+$ and 0^+ $ud\bar{b}\bar{b}$ and $ls\bar{b}\bar{b}$ tetraquark states bound below the lowest two-meson threshold on the E5 ensemble, plotted against r_h in the region where we have data. Coloured bands are the results of correlated fits to Eqs. (10) and (11). The 0^+ results are bolder and slightly offset in r_h for clarity.

V. SUMMARY AND DISCUSSION

In this paper we have revisited the earlier lattice determination of the binding energies of the flavour-antitriplet of doubly-bottom $J^P = 1^+$ tetraquarks reported in Ref. [60], introducing a number of significant improvements and producing results which update and supersede those of Ref. [60]. Relative to the previous study, the new analysis (i) employs expanded sets of interpolating operators for the $ud\bar{b}\bar{b}$ and $ls\bar{b}\bar{b}$ channels, (ii) adds two newly generated, larger-volume ensembles with $m_\pi < 200$ MeV, aimed at reducing possible FV effects, and (iii) rather than using local operators at the sink, as done in Ref. [60], implements the improved box-sink construction of Ref. [56]. As shown in Ref. [56], this construction significantly reduces excited state contamination of the ground-state signal, leading to much longer ground-state effective-mass plateaus, beginning at much earlier Euclidean times, than those obtained in the local-sink analysis of Ref. [60].

Our result for the $I = 0$, $J^P = 1^+$ $ud\bar{b}\bar{b}$ binding, 115(17) MeV, shows some tension with the results of two earlier studies, Refs. [60] and [63], which found 189(10)(3) MeV and 187(18) MeV, respectively, though, as noted above, the former result is superseded by that of the current, improved analysis. Our new result agrees within errors with all other recent lattice results for this channel, with Ref. [61] finding 143(34) MeV, Ref. [62] 128(24)(10) MeV, Ref. [71] 112(13) MeV, Ref. [70] 83(10)(20) MeV and Ref. [73] 100(10) $\left(\begin{smallmatrix} +36 \\ -43 \end{smallmatrix}\right)$ MeV. It is worth noting that among these the physical-point HALQCD result, 83(10)(20) MeV [70], is obtained from a significantly longer physical-point extrapolation (of results with $m_\pi \sim 410$,

575 and 700 MeV) than are the results of Refs. [61, 62, 71, 73] or the current analysis, all of which include ensembles with m_π at least as low as ~ 220 MeV. A potentially large systematic error can arise from the use of NRQCD. It cannot be estimated within our work since we have just one lattice spacing, but a previous study [91] has found it to be of the order of 10 MeV.

We also note that the more recent analysis of Ref. [73] improves on that of Ref. [62], including the “scattering operators” introduced in Ref. [62], and used there only on the sink side, now also on the source side.⁸ Our new result confirms the existence of the deeply-bound $I = 0$, $J^P = 1^+$ $ud\bar{b}\bar{b}$ tetraquark state found in earlier lattice studies and joins other recent lattice analyses [62, 71, 73] in providing a consistent consensus for its binding energy. These results confirm that the state is stable with respect to both strong and electromagnetic interactions, and hence can decay only via the weak interaction. It is thus expected to be narrow, long-lived, and have a large number of exclusive decay modes, each with a small branching fraction, making experimental detection at current facilities extremely challenging (see, e.g., the discussion of this point in Ref. [111]). An alternate, inclusive strategy for detecting the presence of weakly decaying doubly-bottom *hadrons* (via searches for B_c mesons originating from displaced secondary vertices at the LHC) was suggested in Ref. [112]. Such a signal would, in principle, contain contributions from not just the $J^P = 1^+$ $ud\bar{b}\bar{b}$ tetraquark of interest, but also doubly bottom baryons, and hence, on its own, be insufficient to establish the presence of the $ud\bar{b}\bar{b}$ tetraquark signal. It would also, in principle, contain $J^P = 1^+$ $ls\bar{b}\bar{b}$ tetraquark contributions, should the $ls\bar{b}\bar{b}$ state have a binding energy greater than 46 MeV and hence also be able to decay only weakly. In spite of these complications, a search for such displaced B_c vertex events would be of interest in setting an upper bound on the production cross-section for weakly decaying doubly-bottom tetraquark states and determining whether additional efforts to identify, and separate out, the doubly bottom baryon component of the signal would be worth pursuing, all this, of course, provided a good understanding of the resolution of the tail of the impact parameter distribution relative to the primary collision vertex can be achieved.⁹

Our result for the $I = 1/2$, $J^P = 1^+$ $ls\bar{b}\bar{b}$ binding, 47(8) MeV, is (i) significantly lower than the earlier lattice results, 98(7)(3), 87(32) and 86(27)(10) MeV, obtained in the analyses of Refs. [60], [61], and Ref. [74], respectively, but (ii) in good agreement with the more recent results, 46(12) and 30(3) ($^{+31}_{-11}$) MeV, obtained in Refs. [71] and [73]. As noted above, the latter analysis represents an improvement on the earlier analysis of Ref. [74], with the “scattering operators” of the earlier analysis now included at both the source and sink, rather than just the sink. The analysis of Ref. [71] also improves on earlier analyses, employing extended sink-side operators which produce much longer effective-mass plateaus than those found in Refs. [60] and [61].¹⁰ The current analysis provides, via the box-sink construction, a similar improvement for the $J^P = 1^+$ $ls\bar{b}\bar{b}$ ground-state signal. As noted above, our new result, 47(8) MeV, for the binding in this channel also supersedes that obtained in Ref. [60]. We consider the improved features of the analyses of Refs. [71], [73] and the current analysis, and the good agreement of the determinations of the $J^P = 1^+$ $ls\bar{b}\bar{b}$ binding obtained from these improved analyses, to establish the reliability of the lower range of results for the

⁸ In Ref. [62], these scattering operators (the products of pairs of independently zero-momentum-projected single-heavy-meson interpolating operators) were shown to provide improved access to the threshold two-meson BB^* state signal.

⁹ Also worth noting in this context is the observation of double Υ production by CMS [113, 114], which establishes the existence of a non-negligible double $b\bar{b}$ pair production rate, and hence the (at least in principle) possibility of the production of a small number of such weakly decaying doubly bottom hadrons at the LHC.

¹⁰ See Fig. 1 of Ref. [61] and the lower panel of Fig. 1 of Ref. [60] for examples of the short, late-Euclidean-time effective mass $J^P = 1^+$ $ls\bar{b}\bar{b}$ channel plateaus found in those earlier references.

$\text{ls}\bar{\text{b}}\bar{\text{b}}$ binding they produce. The binding is, however, still clearly positive, confirming the strong-interaction-stability of the $J^P = 1^+$ $\text{ls}\bar{\text{b}}\bar{\text{b}}$ state. With the lowest of the two-meson thresholds in this channel, $B_s B^{*+}$, lying only 45.3(3) MeV above $B_s B^+$ threshold, these updated results raise the interesting possibility that the $J^P = 1^+$ $\text{ls}\bar{\text{b}}\bar{\text{b}}$ tetraquark state might lie above the lowest two-heavy-pseudoscalar ($B_s B$) threshold and hence be able to decay electromagnetically to $B_s B$ plus a soft photon. The limited phase space available to such a decay would restrict the maximum relative B_s - B momentum in the $\text{ls}\bar{\text{b}}\bar{\text{b}}$ tetraquark rest frame to relatively low values. In contrast to the case of the $J^P = 1^+$ $\text{ud}\bar{\text{b}}\bar{\text{b}}$ state, where only weak decays are possible and one expects many exclusive decay modes, all with small branching fractions, an electromagnetic $B_s B \gamma$ decay of the $J^P = 1^+$ $\text{ls}\bar{\text{b}}\bar{\text{b}}$ state would be expected to have an essentially 100% branching fraction. While the soft photon from the decay would not be detectable at LHCb, once boosted to the lab frame the B_s and B pair from the decay would be highly collimated and, because of the almost 100% branching fraction, provide a potentially much higher statistics target for an experimental doubly bottom tetraquark search than is the case for any exclusive weak decay of the $\text{ud}\bar{\text{b}}\bar{\text{b}}$ analogue.

We close with a discussion of the $I = 0$, $J^P = 1^+$ and 0^+ $\text{ud}\bar{\text{b}}\bar{\text{c}}$ channels. Though we have not explicitly revisited these channels in this paper, the results of the updated variable-heavy-mass study detailed in Sec. IV B provide some additional qualitative information of relevance to expectations for possible experimental signatures in the bottom-charm sector.

We first note that the longest-distance, one-pion-exchange potentials between the lowest two-meson threshold states are the same for the $I = 0$, $J^P = 1^+$ $\text{ud}\bar{\text{c}}\bar{\text{c}}$, $\text{ud}\bar{\text{b}}\bar{\text{c}}$ and $\text{ud}\bar{\text{b}}\bar{\text{b}}$ channels [3]. At shorter distances, where the variable-heavy-mass results and associated phenomenological fit provide additional qualitative information, the corresponding $\bar{D}\bar{D}^*$, $\bar{D}B^*$ and BB^* two-meson s -wave threshold pairs, in contrast, have access to the heavy-mass-dependent attractive 3_c color Coulomb $\bar{\text{c}}\bar{\text{c}}$, $\bar{\text{c}}\bar{\text{b}}$ and $\bar{\text{b}}\bar{\text{b}}$ interactions, as well as to the other heavy-mass-dependent interactions collectively parametrized by the C_2 term in the phenomenological fit form. The color Coulomb attraction, which is proportional to the heavy-heavy reduced mass, is more attractive in the $\text{ud}\bar{\text{b}}\bar{\text{c}}$ channel than the $\text{ud}\bar{\text{c}}\bar{\text{c}}$ channel, though less attractive than in the $\text{ud}\bar{\text{b}}\bar{\text{b}}$ channel. The shorter-distance, repulsive contribution proportional to C_2 in the $I = 0$, $J^P = 1^+$, $\text{ud}\bar{\text{b}}\bar{\text{h}}$ phenomenological fit form, similarly, becomes less repulsive (hence increasing the binding) as the variable heavy mass, m_h , is increased. If we imagine starting from the very weakly bound T_{cc} state, and changing the \bar{D}^* of the two-meson threshold in that channel slowly to B^* by dialing up the mass of the heavy quark in the vector meson of the two-meson threshold state, we thus expect (i) a small increase in binding (reduced kinetic energy) from long-distance sources due to the larger $B^*\bar{D}$ (c.f. $\bar{D}\bar{D}^*$) reduced mass, and (ii) additional small increases in binding from the short-distance sources just discussed, which become more attractive/less repulsive as the variable heavy mass is increased. These observations provide further support the expectation that a bound tetraquark with binding energy at least somewhat greater than that of the T_{cc} should exist in the $I = 0$, $J^P = 1^+$ $\text{ud}\bar{\text{b}}\bar{\text{c}}$ channel. Recent lattice results restrict how much larger this increased 1^+ $\text{ud}\bar{\text{b}}\bar{\text{c}}$ binding can be, with (i) the results of Refs. [56, 64, 65, 74] indicating at best weak binding¹¹ and favoring results on the low side of the 43 $\binom{+7}{-6}$ $\binom{+24}{-14}$ MeV range reported in Ref. [76], and (ii) the result of the improved, more recent (albeit not-yet-physical-point-extrapolated) $m_\pi \sim 220$ MeV scattering study of Ref. [78], suggesting an even smaller, few to several MeV, value. The preponderance of lattice evidence thus points to the existence of a strong-interaction-stable $I = 0$, $J^P = 1^+$ $\text{ud}\bar{\text{b}}\bar{\text{c}}$ state with binding almost certainly less

¹¹ In the single-ensemble study of Ref. [56], we were easily able to resolve an $\text{ls}\bar{\text{b}}\bar{\text{b}}$ binding of 36 MeV.

than the 46 MeV needed for its mass to lie below $B\bar{D}$ threshold and thus be stable also with respect to electromagnetic decay. The $I = 0$, $J^P = 1^+$ $u\bar{d}\bar{b}\bar{c}$ state is therefore expected to decay electromagnetically.

The lattice scattering study of Ref. [78] also points to the possibility of a bound $I = 0$, $J^P = 0^+$ $u\bar{d}\bar{b}\bar{c}$ state, quoting a binding relative to $B\bar{D}$ threshold of 0.5(9) MeV at $m_\pi \simeq 220$ MeV. If bound at physical m_π , this state would be able to decay only weakly, with multiple exclusive decay modes, each with relatively small branching fraction, representing a challenge for experimental detection. The either very weakly bound or unbound 0^+ result of Ref. [78] is compatible with the results of Refs. [56, 74], which found no sign of a deeply bound state in this channel, though in some tension with the larger $39 \binom{+6}{-4} \binom{+18}{-8}$ MeV 0^+ binding found in the alternate scattering analysis of Ref. [77], where fewer interpolating operators, heavier valence pion masses, but some finer ensembles were employed.

A summary of the above discussion of the $u\bar{d}\bar{b}\bar{c}$ sector is as follows. First, there is now good evidence for the existence of a strong-interaction-stable $I = 0$, $J^P = 1^+$ $u\bar{d}\bar{b}\bar{c}$ partner of the T_{cc} with binding small enough to allow it to decay electromagnetically. Second, though it is clear that a bound $I = 0$, $J^P = 0^+$ $u\bar{d}\bar{b}\bar{c}$ tetraquark would exist were the charm-quark mass to be sufficiently heavier than it is in nature, without a $J^P = 0^+$ analogue of the T_{cc} to anchor the discussion it is not yet clear whether binding survives in this channel at physical m_c and m_π . If the $J^P = 0^+$ state is *not* bound, then the 1^+ state should decay essentially 100% of the time to $B\bar{D}\gamma$, producing highly collimated $B\text{-}\bar{D}$ pairs in the lab frame with a narrow range of invariant masses lying between $m_B + m_D$ and the 1^+ tetraquark mass. If, in contrast, the $J^P = 0^+$ state *is* bound, the 1^+ state will decay electromagnetically to a soft photon plus the 0^+ state as well as to $B\bar{D}\gamma$. With at most weak 0^+ binding, the branching fraction of the $B\bar{D}\gamma$ mode should, however, still be sizeable. While the multiple small branching fraction exclusive modes of the weak decay of the 0^+ state in this scenario will make detecting not just the production of the 0^+ state itself, but also the 0^+ -plus-soft photon decay branch of the 1^+ state experimentally challenging, the $B\bar{D}\gamma$ branch will have the same potentially useful, statistically enhanced signal as in the scenario where the 0^+ state is unbound.

ACKNOWLEDGEMENTS

The authors wish to thank G. P. Lepage for considerable input and advice regarding correlator fitting with his software (described in text). WP, RL and KM are supported by grants from the Natural Sciences and Engineering Research Council of Canada. AF acknowledges support by the National Science and Technology Council of Taiwan under grant 111-2112-M-A49-018-MY2. All computations were carried out using an allocations as part of the Digital Research Alliance of Canada on the Niagara supercomputer at Scinet.

-
- [1] J. Ader, J. Richard, and P. Taxil, Phys. Rev. D **25**, 2370 (1982).
 - [2] L. Heller and J. Tjon, Phys. Rev. D **35**, 969 (1987).
 - [3] A. V. Manohar and M. B. Wise, Nucl. Phys. B **399**, 17 (1993), arXiv:hep-ph/9212236.
 - [4] D. G. Richards, D. K. Sinclair, and D. W. Sivers, Phys. Rev. **D42**, 3191 (1990).
 - [5] A. Mihaly, H. R. Fiebig, H. Markum, and K. Rabitsch, Phys. Rev. **D55**, 3077 (1997).

- [6] A. M. Green and P. Pennanen, *Phys. Rev.* **C57**, 3384 (1998), arXiv:hep-lat/9804003 [hep-lat].
- [7] C. Stewart and R. Koniuk, *Phys. Rev.* **D57**, 5581 (1998), arXiv:hep-lat/9803003 [hep-lat].
- [8] C. Michael and P. Pennanen (UKQCD), *Phys. Rev.* **D60**, 054012 (1999), arXiv:hep-lat/9901007 [hep-lat].
- [9] P. Pennanen, C. Michael, and A. M. Green (UKQCD), *Nucl. Phys. Proc. Suppl.* **83**, 200 (2000), arXiv:hep-lat/9908032 [hep-lat].
- [10] M. S. Cook and H. R. Fiebig, (2002), arXiv:hep-lat/0210054 [hep-lat].
- [11] T. Doi, T. T. Takahashi, and H. Suganuma, *AIP Conf. Proc.* **842**, 246 (2006), arXiv:hep-lat/0601008.
- [12] W. Detmold, K. Orginos, and M. J. Savage, *Phys. Rev.* **D76**, 114503 (2007), arXiv:hep-lat/0703009 [HEP-LAT].
- [13] J. Carlson, L. Heller, and J. Tjon, *Phys. Rev. D* **37**, 744 (1988).
- [14] S. Zouzou, B. Silvestre-Brac, C. Gignoux, and J. Richard, *Z. Phys. C* **30**, 457 (1986).
- [15] H. J. Lipkin, *Phys. Lett. B* **172**, 242 (1986).
- [16] B. Silvestre-Brac and C. Semay, *Z. Phys. C* **57**, 273 (1993).
- [17] C. Semay and B. Silvestre-Brac, *Z. Phys. C* **61**, 271 (1994).
- [18] S. Pepin, F. Stancu, M. Genovese, and J. Richard, *Phys. Lett. B* **393**, 119 (1997), arXiv:hep-ph/9609348.
- [19] D. Brink and F. Stancu, *Phys. Rev. D* **57**, 6778 (1998).
- [20] J. Vijande, F. Fernandez, A. Valcarce, and B. Silvestre-Brac, *Eur. Phys. J. A* **19**, 383 (2004), arXiv:hep-ph/0310007.
- [21] D. Janc and M. Rosina, *Few Body Syst.* **35**, 175 (2004), arXiv:hep-ph/0405208.
- [22] J. Vijande, E. Weissman, A. Valcarce, and N. Barnea, *Phys. Rev. D* **76**, 094027 (2007), arXiv:0710.2516 [hep-ph].
- [23] D. Ebert, R. Faustov, V. Galkin, and W. Lucha, *Phys. Rev. D* **76**, 114015 (2007), arXiv:0706.3853 [hep-ph].
- [24] M. Zhang, H. Zhang, and Z. Zhang, *Commun. Theor. Phys.* **50**, 437 (2008), arXiv:0711.1029 [nucl-th].
- [25] J. Vijande, A. Valcarce, and N. Barnea, *Phys. Rev. D* **79**, 074010 (2009), arXiv:0903.2949 [hep-ph].
- [26] Y. Yang, C. Deng, J. Ping, and T. Goldman, *Phys. Rev. D* **80**, 114023 (2009).
- [27] T. Carames, A. Valcarce, and J. Vijande, *Phys. Lett. B* **699**, 291 (2011).
- [28] R. R. Silbar and T. Goldman, *Int. J. Mod. Phys. E* **23**, 1450091 (2014), arXiv:1304.5480 [nucl-th].
- [29] M. Karliner and J. L. Rosner, *Phys. Rev. Lett.* **119**, 202001 (2017), arXiv:1707.07666 [hep-ph].
- [30] T. F. Caramés, J. Vijande, and A. Valcarce, *Phys. Rev. D* **99**, 014006 (2019), arXiv:1812.08991 [hep-ph].
- [31] C. Deng, H. Chen, and J. Ping, *Eur. Phys. J. A* **56**, 9 (2020), arXiv:1811.06462 [hep-ph].
- [32] W. Park, S. Noh, and S. H. Lee, *Nucl. Phys. A* **983**, 1 (2019), arXiv:1809.05257 [nucl-th].
- [33] G. Yang, J. Ping, and J. Segovia, *Phys. Rev. D* **101**, 014001 (2020), arXiv:1911.00215 [hep-ph].
- [34] E. Hernández, J. Vijande, A. Valcarce, and J.-M. Richard, *Phys. Lett. B* **800**, 135073 (2020), arXiv:1910.13394 [hep-ph].
- [35] Y. Tan, W. Lu, and J. Ping, *Eur. Phys. J. Plus* **135**, 716 (2020), arXiv:2004.02106 [hep-ph].
- [36] Q.-F. Lü, D.-Y. Chen, and Y.-B. Dong, *Phys. Rev. D* **102**, 034012 (2020), arXiv:2006.08087 [hep-ph].

- [37] J.-B. Cheng, S.-Y. Li, Y.-R. Liu, Z.-G. Si, and T. Yao, *Chin. Phys. C* **45**, 043102 (2021), arXiv:2008.00737 [hep-ph].
- [38] Q. Meng, E. Hiyama, A. Hosaka, M. Oka, P. Gubler, K. U. Can, T. T. Takahashi, and H. S. Zong, *Phys. Lett. B* **814**, 136095 (2021), arXiv:2009.14493 [nucl-th].
- [39] S. Noh, W. Park, and S. H. Lee, *Phys. Rev. D* **103**, 114009 (2021), arXiv:2102.09614 [hep-ph].
- [40] S. Ohkoda, Y. Yamaguchi, S. Yasui, K. Sudoh, and A. Hosaka, *Phys. Rev. D* **86**, 034019 (2012), arXiv:1202.0760 [hep-ph].
- [41] A. Czarnecki, B. Leng, and M. Voloshin, *Phys. Lett. B* **778**, 233 (2018), arXiv:1708.04594 [hep-ph].
- [42] E. J. Eichten and C. Quigg, *Phys. Rev. Lett.* **119**, 202002 (2017), arXiv:1707.09575 [hep-ph].
- [43] E. Braaten, L.-P. He, and A. Mohapatra, *Phys. Rev. D* **103**, 016001 (2021), arXiv:2006.08650 [hep-ph].
- [44] M. A. Shifman, A. Vainshtein, and V. I. Zakharov, *Nucl. Phys. B* **147**, 385 (1979).
- [45] M. A. Shifman, A. Vainshtein, and V. I. Zakharov, *Nucl. Phys. B* **147**, 448 (1979).
- [46] F. S. Navarra, M. Nielsen, and S. H. Lee, *Phys. Lett. B* **649**, 166 (2007), arXiv:hep-ph/0703071.
- [47] M.-L. Du, W. Chen, X.-L. Chen, and S.-L. Zhu, *Phys. Rev. D* **87**, 014003 (2013), arXiv:1209.5134 [hep-ph].
- [48] W. Chen, T. Steele, and S.-L. Zhu, *Phys. Rev. D* **89**, 054037 (2014), arXiv:1310.8337 [hep-ph].
- [49] Z.-G. Wang, *Acta Phys. Polon. B* **49**, 1781 (2018), arXiv:1708.04545 [hep-ph].
- [50] S. Agaev, K. Azizi, B. Barsbay, and H. Sundu, *Phys. Rev. D* **99**, 033002 (2019), arXiv:1809.07791 [hep-ph].
- [51] S. S. Agaev, K. Azizi, and H. Sundu, *Nucl. Phys. B* **951**, 114890 (2020), arXiv:1905.07591 [hep-ph].
- [52] S. Agaev, K. Azizi, and H. Sundu, *Phys. Rev. D* **100**, 094020 (2019), arXiv:1907.04017 [hep-ph].
- [53] L. Tang, B.-D. Wan, K. Maltman, and C.-F. Qiao, *Phys. Rev. D* **101**, 094032 (2020), arXiv:1911.10951 [hep-ph].
- [54] Q.-N. Wang and W. Chen, *Eur. Phys. J. C* **80**, 389 (2020), arXiv:2002.04243 [hep-ph].
- [55] S. S. Agaev, K. Azizi, B. Barsbay, and H. Sundu, *Chin. Phys. C* **45**, 013105 (2021), arXiv:2002.04553 [hep-ph].
- [56] R. J. Hudspith, B. Colquhoun, A. Francis, R. Lewis, and K. Maltman, *Phys. Rev. D* **102**, 114506 (2020), arXiv:2006.14294 [hep-lat].
- [57] P. Bicudo, K. Cichy, A. Peters, and M. Wagner, *Phys. Rev. D* **93**, 034501 (2016), arXiv:1510.03441 [hep-lat].
- [58] P. Bicudo, J. Scheunert, and M. Wagner, *Phys. Rev. D* **95**, 034502 (2017), arXiv:1612.02758 [hep-lat].
- [59] P. Bicudo, M. Cardoso, A. Peters, M. Pflaumer, and M. Wagner, *Phys. Rev. D* **96**, 054510 (2017), arXiv:1704.02383 [hep-lat].
- [60] A. Francis, R. J. Hudspith, R. Lewis, and K. Maltman, *Phys. Rev. Lett.* **118**, 142001 (2017), arXiv:1607.05214 [hep-lat].
- [61] P. Junnarkar, N. Mathur, and M. Padmanath, *Phys. Rev. D* **99**, 034507 (2019), arXiv:1810.12285 [hep-lat].
- [62] L. Leskovec, S. Meinel, M. Pflaumer, and M. Wagner, *Phys. Rev. D* **100**, 014503 (2019), arXiv:1904.04197 [hep-lat].
- [63] P. Mohanta and S. Basak, *Phys. Rev. D* **102**, 094516 (2020), arXiv:2008.11146 [hep-lat].

- [64] M. Pflaumer, L. Leskovec, S. Meinel, and M. Wagner, in *Asia-Pacific Symposium for Lattice Field Theory* (2020) arXiv:2009.10538 [hep-lat].
- [65] M. Pflaumer, L. Leskovec, S. Meinel, and M. Wagner, PoS **LATTICE2021**, 392 (2022), arXiv:2108.10704 [hep-lat].
- [66] M. Wagner, C. Alexandrou, J. Finkenrath, T. Leontiou, S. Meinel, and M. Pflaumer, PoS **LATTICE2022**, 270 (2023), arXiv:2210.09281 [hep-lat].
- [67] M. Pflaumer, C. Alexandrou, J. Finkenrath, T. Leontiou, S. Meinel, and M. Wagner, PoS **LATTICE2022**, 075 (2023), arXiv:2211.00951 [hep-lat].
- [68] B. Colquhoun, A. Francis, R. J. Hudspith, R. Lewis, and K. Maltman, PoS **LATTICE2021**, 144 (2022).
- [69] B. Colquhoun, A. Francis, R. Hudspith, R. Lewis, and K. Maltman, Rev. Mex. Fis. Suppl. **3**, 0308044 (2022).
- [70] T. Aoki, S. Aoki, and T. Inoue, Phys. Rev. D **108**, 054502 (2023), arXiv:2306.03565 [hep-lat].
- [71] R. J. Hudspith and D. Mohler, Phys. Rev. D **107**, 114510 (2023), arXiv:2303.17295 [hep-lat].
- [72] L. Mueller, P. Bicudo, M. Krstic Marinkovic, and M. Wagner (2023) arXiv:2312.17060 [hep-lat].
- [73] C. Alexandrou, J. Finkenrath, T. Leontiou, S. Meinel, M. Pflaumer, and M. Wagner, (2024), arXiv:2404.03588 [hep-lat].
- [74] S. Meinel, M. Pflaumer, and M. Wagner, Phys. Rev. D **106**, 034507 (2022), arXiv:2205.13982 [hep-lat].
- [75] N. Mathur and M. Padmanath, PoS **LATTICE2021**, 443 (2022), arXiv:2111.01147 [hep-lat].
- [76] M. Padmanath, A. Radhakrishnan, and N. Mathur, (2023), arXiv:2307.14128 [hep-lat].
- [77] A. Radhakrishnan, M. Padmanath, and N. Mathur, (2024), arXiv:2404.08109 [hep-lat].
- [78] C. Alexandrou, J. Finkenrath, T. Leontiou, S. Meinel, M. Pflaumer, and M. Wagner, (2023), arXiv:2312.02925 [hep-lat].
- [79] R. Aaij *et al.* (LHCb), Nature Phys. **18**, 751 (2022), arXiv:2109.01038 [hep-ex].
- [80] R. Aaij *et al.* (LHCb), Nature Commun. **13**, 3351 (2022), arXiv:2109.01056 [hep-ex].
- [81] G. K. C. Cheung, C. E. Thomas, J. J. Dudek, and R. G. Edwards (Hadron Spectrum), JHEP **11**, 033 (2017), arXiv:1709.01417 [hep-lat].
- [82] A. Francis, R. J. Hudspith, R. Lewis, and K. Maltman, Phys. Rev. D **99**, 054505 (2019), arXiv:1810.10550 [hep-lat].
- [83] M. Padmanath and S. Prelovsek, Phys. Rev. Lett. **129**, 032002 (2022), arXiv:2202.10110 [hep-lat].
- [84] S. Chen, C. Shi, Y. Chen, M. Gong, Z. Liu, W. Sun, and R. Zhang, Phys. Lett. B **833**, 137391 (2022), arXiv:2206.06185 [hep-lat].
- [85] Y. Lyu, S. Aoki, T. Doi, T. Hatsuda, Y. Ikeda, and J. Meng, Phys. Rev. Lett. **131**, 161901 (2023), arXiv:2302.04505 [hep-lat].
- [86] E. Ortiz-Pacheco, S. Collins, L. Leskovec, M. Padmanath, and S. Prelovsek, (2023), 10.22323/1.453.0052, arXiv:2312.13441 [hep-lat].
- [87] S. Collins, A. Nefediev, M. Padmanath, and S. Prelovsek, (2024), arXiv:2402.14715 [hep-lat].
- [88] T. Whyte, D. J. Wilson, and C. E. Thomas, (2024), arXiv:2405.15741 [hep-lat].
- [89] S. Aoki and T. Aoki, PoS **LATTICE2022**, 049 (2023), arXiv:2212.00202 [hep-lat].
- [90] R. J. Hudspith (RBC, UKQCD), Comput. Phys. Commun. **187**, 115 (2015), arXiv:1405.5812 [hep-lat].
- [91] R. J. Hudspith and D. Mohler, Phys. Rev. D **106**, 034508 (2022), arXiv:2112.01997 [hep-lat].
- [92] S. Aoki *et al.* (PACS-CS), Phys. Rev. D **79**, 034503 (2009), arXiv:0807.1661 [hep-lat].

- [93] S. Aoki *et al.* (PACS-CS), Phys. Rev. D **81**, 074503 (2010), arXiv:0911.2561 [hep-lat].
- [94] S. Aoki *et al.* (PACS-CS), Phys. Rev. D **79**, 034503 (2009), arXiv:0807.1661 [hep-lat].
- [95] C. B. Lang, L. Leskovec, D. Mohler, S. Prelovsek, and R. M. Woloshyn, Phys. Rev. D **90**, 034510 (2014), arXiv:1403.8103 [hep-lat].
- [96] Y. Namekawa *et al.* (PACS-CS), Phys. Rev. D **84**, 074505 (2011), arXiv:1104.4600 [hep-lat].
- [97] M. Luscher and S. Schaefer, Comput. Phys. Commun. **184**, 519 (2013), arXiv:1206.2809 [hep-lat].
- [98] <http://luscher.web.cern.ch/luscher/openQCD/>.
- [99] M. Luscher, JHEP **07**, 081 (2007), arXiv:0706.2298 [hep-lat].
- [100] M. Hasenbusch and K. Jansen, Nucl. Phys. B **659**, 299 (2003), arXiv:hep-lat/0211042.
- [101] R. C. Brower, T. Ivanenko, A. R. Levi, and K. N. Orginos, Nucl. Phys. B **484**, 353 (1997), arXiv:hep-lat/9509012.
- [102] M. A. Clark and A. D. Kennedy, Nucl. Phys. B Proc. Suppl. **129**, 850 (2004), arXiv:hep-lat/0309084.
- [103] R. Frezzotti and K. Jansen, Nucl. Phys. B **555**, 395 (1999), arXiv:hep-lat/9808011.
- [104] G. P. Lepage, B. Clark, C. T. H. Davies, K. Hornbostel, P. B. Mackenzie, C. Morningstar, and H. Trotter (HPQCD), Nucl. Phys. B Proc. Suppl. **106**, 12 (2002), arXiv:hep-lat/0110175.
- [105] P. Lepage, “gplepage/corrfitter: corrfitter version 8.2,” (2021).
- [106] P. Lepage and C. Gohlke, “gplepage/lqfit: lqfit version 13.0.1,” (2023).
- [107] P. Lepage, C. Gohlke, and D. Hackett, “gplepage/gvar: gvar version 11.11.11,” (2023).
- [108] R. J. Dowdall, C. T. H. Davies, R. R. Horgan, G. P. Lepage, C. J. Monahan, J. Shigemitsu, and M. Wingate, Phys. Rev. D **100**, 094508 (2019), arXiv:1907.01025 [hep-lat].
- [109] G. D’Agostini, Nuclear Instruments and Methods in Physics Research Section A: Accelerators, Spectrometers, Detectors and Associated Equipment **346**, 306 (1994).
- [110] R. L. Workman and Others (Particle Data Group), PTEP **2022**, 083C01 (2022).
- [111] S. Blusk, *Beyond T_{cc} : T_{bc} and T_{bb}* , LHCb Online Mini-Workshop: T_{cc} and Beyond, September 14, 2021.
- [112] T. Gershon and A. Poluektov, JHEP **01**, 019 (2019), arXiv:1810.06657 [hep-ph].
- [113] V. Khachatryan *et al.* (CMS), JHEP **05**, 013 (2017), arXiv:1610.07095 [hep-ex].
- [114] A. M. Sirunyan *et al.* (CMS), Phys. Lett. B **808**, 135578 (2020), arXiv:2002.06393 [hep-ex].